Seismic Oil of Olay: wrinkle reduction on 3D source ensembles

David C Henley

ABSTRACT

We have shown in other work that interferometric principles can be used to remove effects of the near-surface layers from seismic reflection data. Our method, raypath interferometry, has been successfully applied to several 2D seismic lines, and has proven comparable or superior to conventional surface correction methods, particularly for converted wave data, or for any dataset where surface-consistency is not satisfied, or non-stationary surface correction is required. It has also been demonstrated that raypath interferometry can be applied to small 3D seismic surveys, but that the processing burden makes the approach unattractive for larger surveys.

We show here the results of experimental pre-processing, based on interferometric principles, applied to large 3D source gathers in which we attempt to remove, at least partially, the near-surface effects at the receivers within a 3D array, independently for each shot. We envision this as the possible first step of a two-part process, in which the second step removes near-surface effects between source locations prior to CMP stacking or imaging. We explore three interferometric approaches to removing near-surface effects from receiver locations within source gathers. Just as the application of Oil of Olay attempts to reduce facial wrinkles on mature adults, the application of interferometry attempts to remove the 'wrinkles' due to near-surface effects from reflections on 3D seismic source gathers.

INTRODUCTION

Arguably, one of the most difficult processes in preparing seismic data for CMP stacking and imaging is removing the effects of the unconsolidated, highly variable near-surface layer; time delays, phase distortion, and scattered events, all of which affect otherwise clean reflection events from deep layer boundaries. Many approaches have been explored for dealing with this problem, particularly including the many methods of 'static correction', which attempt to derive and apply time shifts, and sometimes phase corrections, to each input seismic trace in order to align the reflection events on them prior to CMP stacking and other imaging processes. On clean PP reflection data with a low-velocity surface layer and low level of additive noise, these methods are generally successful; but they begin to fail on noisy data, in regions with high-velocity surface layers, and particularly on the shear wave leg of PS (converted wave) data, where a non-stationary correction approach is required (Cova et al, 2013, 2014, 2015a, 2015b, 2017).

Raypath interferometry

We began, several years ago, to develop methods for removing the effects of the near-surface layer which do not rely on specific time 'picks' of reflection or refraction events, and which do not use the conventional method of time-shifting whole seismic traces to apply corrections. Obtaining time picks for seismic events, whether using cross-correlations or visual methods, is a non-linear, often subjective process which is inherently vulnerable to error in the process and susceptible to noise in the data, while

time-shifting traces is a simplified operation based on data assumptions that are often violated, such as surface-consistency and single discrete reflection arrivals (Henley, 2008, 2012a, 2012b, 2014a). Beginning with the concept of 'statics deconvolution' (Henley, 2004), and later introducing the concept of applying corrections in the 'raypath direction' (Henley, 2005), we developed the process known as 'raypath interferometry'. In this technique, the near-surface corrections are derived and applied, via an interferometric process, in the 'common raypath' domain. Discrete picks are never used, and time shifts never explicitly applied. The usual restrictive constraints associated with conventional statics correction, surface-consistency and single-arrival reflection events, are special cases of our more relaxed general constraints, 'raypath consistency' and the 'arrival distribution wavelet'. Hence, datasets which can be successfully corrected with conventional methods can also be corrected via the less constrained raypath interferometry (Henley, 2012a, 2012b). However, datasets which violate conventional statics assumptions, such as high-velocity surface layers and converted wave surveys, can only be successfully processed by a more general procedure like raypath interferometry (Henley, 2012a, Cova et al, 2013, 2014).

3D complications

We have showed that raypath interferometry can be successfully applied to 2D data, and that its concepts can be extended to 3D data, as well (Henley, 2015, 2016a, 2016b, 2017a, 2017b). The extension into 3D is not totally straightforward, but it has been demonstrated successfully. The biggest problem encountered in the 3D implementation is the transformation of the original X/T data into a 'raypath' domain and back. We had developed a radial trace (RT) transform many years ago in ProMAX (SeisSpace) which was suitable for the forward/inverse RT transform for data that were confined strictly to a 2D plane, because we incorporated a shortcut for replacing trace headers in the output trace ensemble during RT transform inversion. Any departure from 2D, however, such as a source position displaced laterally from the receiver line, renders a distorted inverse RT transform, unsuitable for further processing. At the time we were first exploring raypath interferometry in 3D, we had only this early, unsuitable RT transform algorithm, so we chose the Tau-P transform as an alternative method to move X/T data to a raypath domain and back (Cova et al, 2014, 2015a). When the aperture and trace increment for the Tau-P transform are chosen to allow sufficient lateral resolution for a high-fidelity forward/inverse Tau-P transform, the Tau-P transform itself becomes quite large, requiring sometimes two orders of magnitude more storage than the original X/T trace gather. For even a relatively small 3D survey, intermediate file size for processing becomes a significant concern with this approach. We demonstrated success with raypath interferometry on the 1995 Blackfoot 3D 3C survey (Henley, 2016a, 2017a, 2017b), but the process was tedious.

In a companion report (Henley, 2018), we document the problem with our original RT transform and describe the repair that has been applied to our software module. This removes at least part of the difficulty with working with 3D data, since storage for the RT transform of a typical X/T gather needs to be only two or three times as large as the X/T storage. Nevertheless, for very large 3D surveys, full raypath interferometry will always be tedious, since the process, by its very nature, is an areal process, requiring a very large portion of any given survey to be accessible simultaneously.

A more limited approach

Ideally, we would like to apply the full raypath interferometry approach to a complete 3D data set in order to remove the effects of the near-surface layer from both source and receiver locations. Many 3D surveys, however, are so large that it would be impractical to attempt this approach—the best compromise might be to apply the method to a subset, or 'patch' of a larger 3D survey, then to somehow blend the 'patches' back together.

Here, we consider that a patch might be as small as a single-fold source ensemble, since such a trace gather may still consist of thousands of traces, sampling a significant area. Hence, if we can interferometrically correct each individual source gather for near-surface effects at the receiver locations within the gather, we can subsequently compare and correlate two receiver-corrected source gathers by registering stacked portions of the estimated wavefield for shared receiver lines. This should allow us to derive and apply a convolution operator to remove the surface function difference between the two source gathers sharing receiver lines.

A procedure by which we would reconcile 3D source ensembles after applying receiver corrections has not been clearly identified, other than the vague description above. We restrict ourselves in this study to taking the 'wrinkles' out of individual 3D source ensembles due to receiver-side near-surface effects. We explore three different schemes for interferometrically correcting an individual source gather, all approximate because of geometric compromises involved in collecting significant ensembles of traces from a single-fold 3D source gather:

- 2D approximately surface-consistent
- 3D approximately surface-consistent
- 3D approximately raypath-consistent.

TESTING THE CONCEPT

We selected a single 3D source gather consisting of 32 receiver lines and containing nearly 6700 traces for our experiments. Data quality was reasonable, but noise levels, particularly for the traces furthest from the source were high. Essentially, we regarded this single source gather as a small single-fold 3D survey and proceeded to apply methods we devised for a standard 3D land survey, while recognizing that one of our usual data dimensions, source position, could not be used for sorting data into configurations useful for interferometry.

Geometry considerations

A 3D source gather, while in essence a legitimate single-fold 3D survey on its own, has a much more limited distribution of geometric trace attributes than a full, multi-fold 3D survey. This limits the formation of legitimate common-attribute trace ensembles for use in data comparisons. The most obvious and useful common-attribute ensembles within a typical 3D source gather are the receiver-line ensembles, each of which is similar to a single-fold 2D survey. These ensembles have the finest and most uniform trace spacing, and capture both surface waves and reflection events with the least spatial

aliasing (Henley, 2007). Figure 1 illustrates the areal distribution of seismic traces in receiver line gathers. Our first interferometry demonstration utilizes the close proximity of traces organized in receiver line gathers to correct the near-surface effects in individual gathers.

Two other trace geometry attributes which prove useful for forming meaningful ensembles are the source-receiver offset distance and the source-receiver azimuth. For the former, we can envision collecting traces in concentric rings centred on the source point, as shown in Figure 2, or in half-rings, if we assign an arithmetic sign to the offsets, depending upon which side of a perpendicular line projected through the source point the traces lie. From Figure 2, we can see that the offset rings may need to be fairly wide in order to capture enough traces to form a meaningful ensemble. In this context, a 'meaningful' ensemble is one in which the collected traces will be 'similar' to one another in some sense identifiable with their common parameter. Individual reflection events on common-offset ensembles, for example, are often assumed to be associated with a relatively narrow range of raypath angles.

If we gather traces according to common source-receiver azimuth, they will lie in wedge-shaped segments whose apexes lie at the source point, as shown in Figure 3. As for the common-offset bins described above, the azimuth bins may need to be relatively wide in order to capture enough traces for a meaningful ensemble, particularly since the distribution of traces within an azimuth segment may be quite irregular. A 'meaningful' common-azimuth ensemble will be one where the reflections are assumed to lie relatively close to a 2D vertical plane aligned with the azimuth.

The geometry associated with azimuth and offset means that trace characteristics associated with those attributes are in some sense approximately orthogonal, and that we can achieve areal smoothing by applying 2D smoothing along each of the azimuth and offset trace coordinates separately and consecutively.

Regardless of what geometric attributes we use to form ensembles for interferometry, our 'before' and 'after' data comparisons will always be between comparable receiver line ensembles, since, as stated before, these are the best spatially sampled trace groups in a 3D source ensemble, and they show both reflections and any residual surface waves.

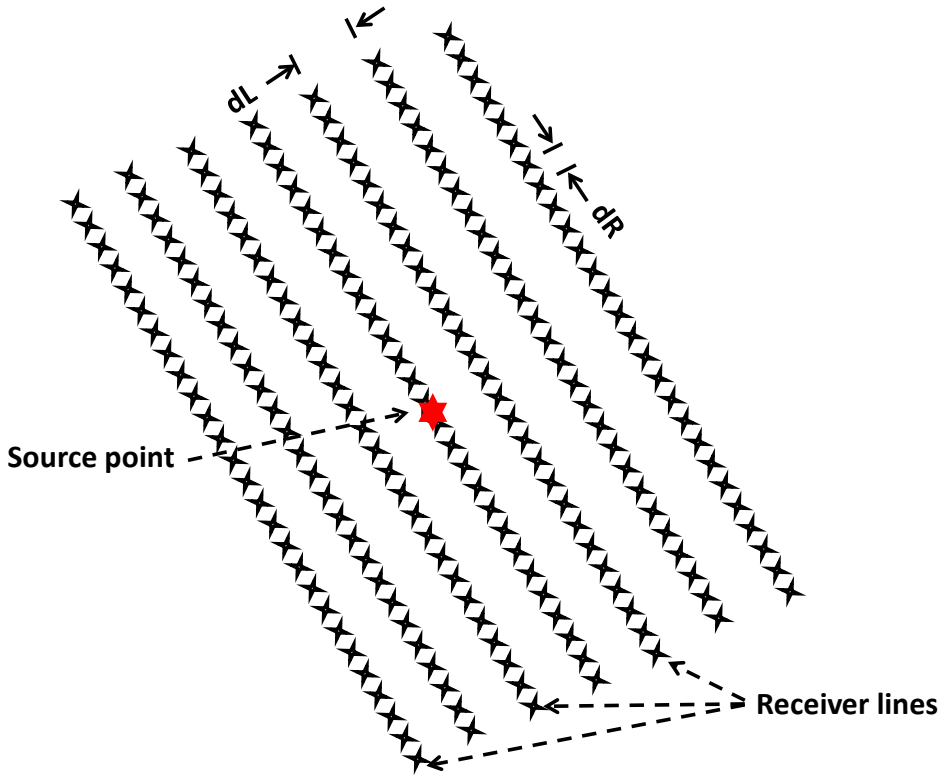

FIG. 1. Schematic of the geometry of a typical source gather for 3D land seismic acquisition. The spacing between receiver lines, dL, is typically several times the spacing between receivers, dR.

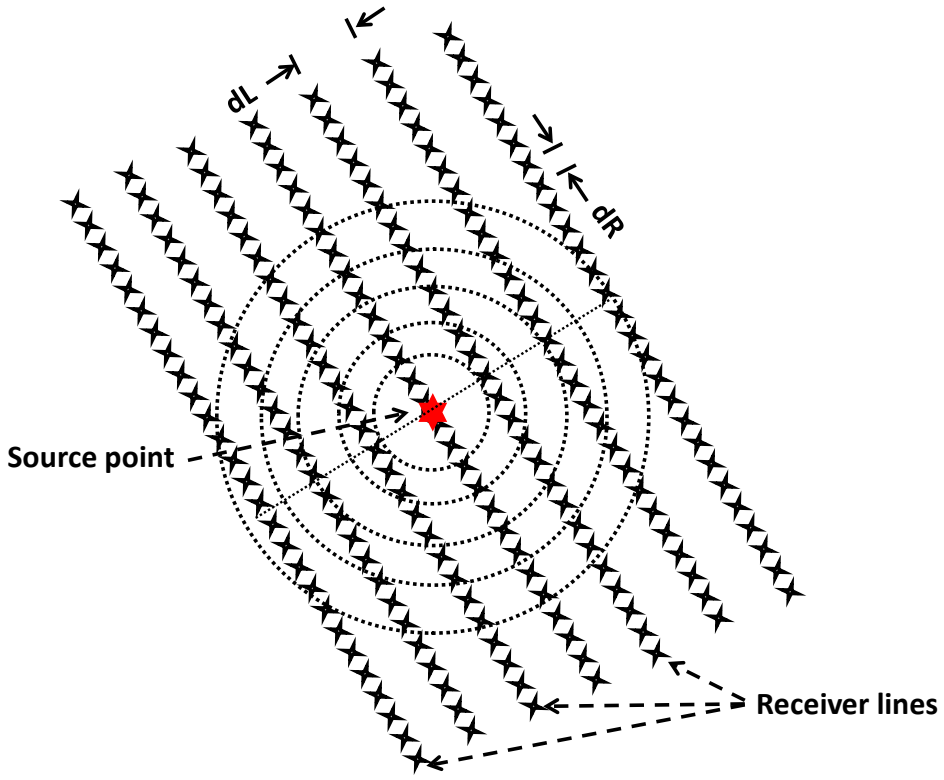

FIG. 2. Schematic showing 3D land acquisition geometry overlaid with rings (or half-rings) showing the shape of bins required for 'constant offset' trace gathers. The spatial distribution of traces within these bins is quite irregular, unless further organized, perhaps by azimuth.

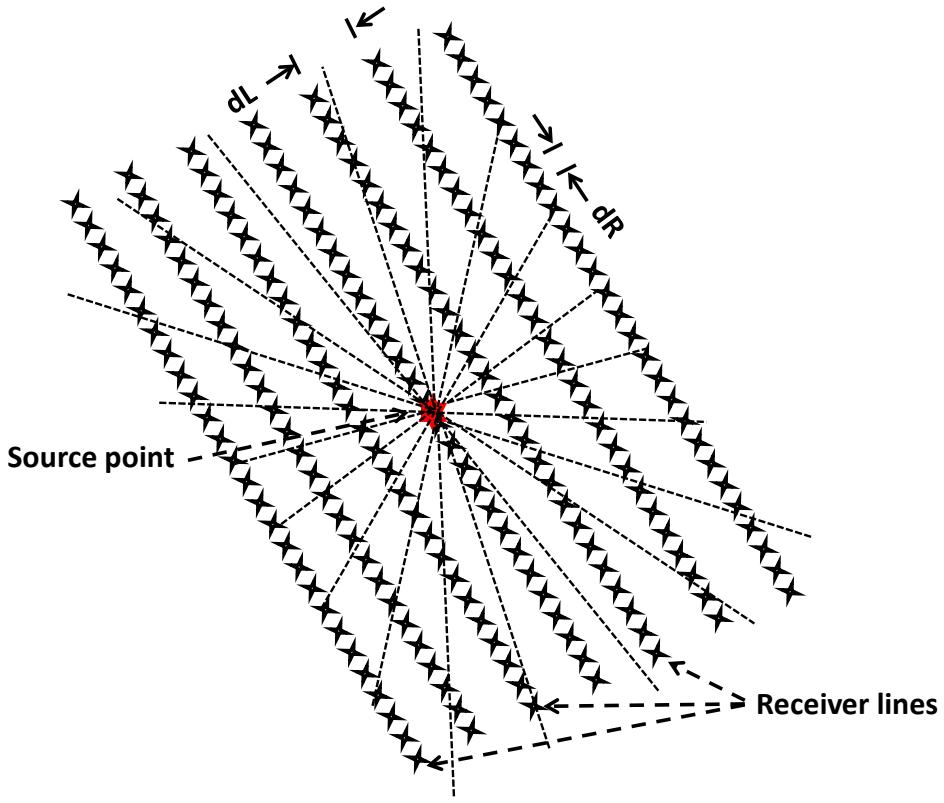

FIG. 3. Schematic showing 3D land acquisition geometry overlaid with sectors showing the shape of bins required for 'constant azimuth' trace gathers. The offset distribution of traces within these bins is irregular, unless further organized, perhaps by offset.

Interferometry 101

The process to which we refer as interferometry is shown schematically in Figure 4, where we portray an optical analog experiment familiar from undergraduate physics lab experiments. In this schematic, a wavefield or wavefront impinges simultaneously on a smooth, undisturbed medium and an irregular medium. The wavefield emerging from the undisturbed medium is cross-correlated with the disturbed wavefield emerging from the irregular medium, and the cross-correlations are used to apply corrections to the disturbed wavefield to remove the distortions caused by the irregular medium. While in the optical lab, we measure the 'undisturbed' wavefield directly, in our seismic application we must always estimate the wavefield from the data, which we do by various smoothing and/or filtering algorithms (Henley, 2012a, 2014b), assuming the irregularities which we are trying to remove are random and of much smaller scale than the smoothing operators. While the process we show schematically in Figure 4 is 2D, extension to 3D is very straightforward in that the wavefront becomes two-dimensional, and smoothing in two spatial directions (not necessarily orthogonal) is needed to estimate the undisturbed wavefield. Cross-correlation with the measured wavefield then takes place along these two dimensions, as does the resulting convolutional correction process. In what follows, we will apply the concept in Figure 4, first in the 2D sense, then in an approximate 3D sense:

- Apply 2D interferometry to individual 3D receiver line ensembles
- Apply 3D interferometry to ensembles sorted by azimuth bin and receiver line
- Apply 3D interferometry to ensembles sorted by azimuth bin and offset, transformed to Tau-P raypath domain.

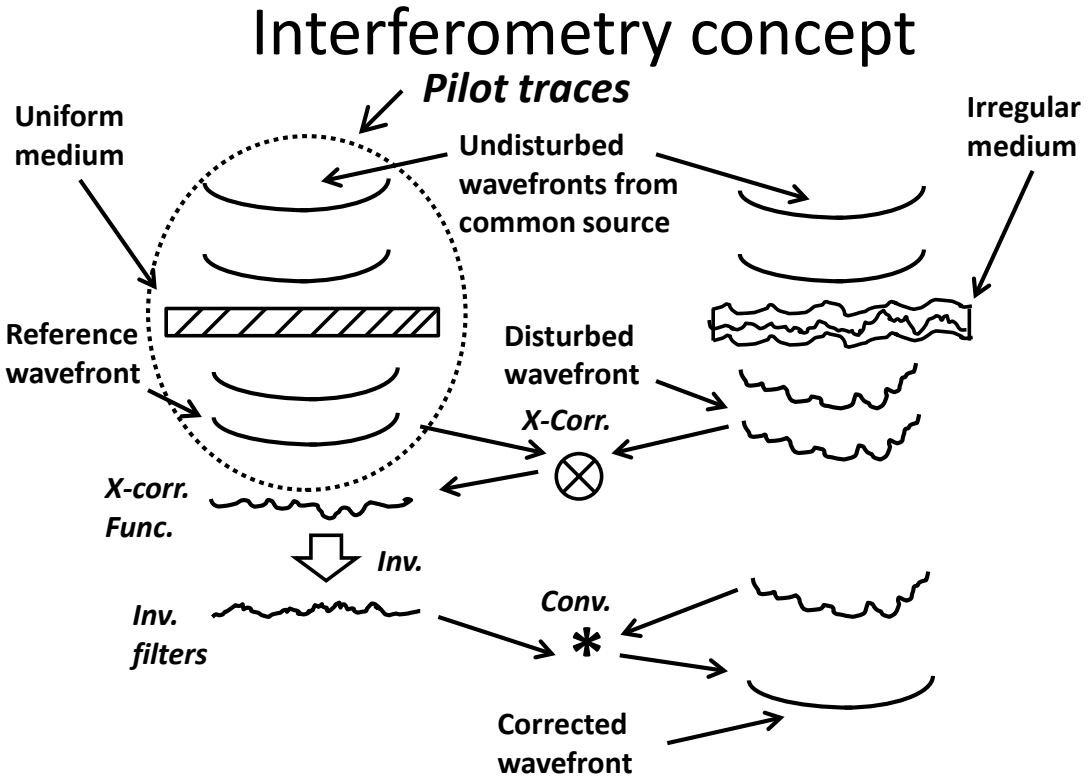

FIG. 4. Schematic showing the interferometric principle we use to remove the near-surface-caused irregularities in reflections.

PROCESSING DETAILS

During our early examination of our trial 3D source gather, we determined that the data were contaminated with a strong system of surface waves, which needed to be attenuated before trying to enhance reflections by removing near-surface effects. To illustrate this problem, we show in Figure 5 receiver line ensemble 17, located near the centre of the source ensemble, after application of AGC. Surface waves dominate this display; reflections are only visible outside the central noise cone. We have showed in other work that radial trace domain filtering can be effectively applied to 3D receiver line gathers (Henley, 2007), and we demonstrate here by applying a radial trace fan filter to the receiver line gather to yield the result in Figure 6. Here, the energy in the noise cone is significantly reduced relative to the reflections, and fragments of reflections can now be seen even inside the noise cone. We applied radial trace fan filters to all receiver lines in the source gather. The filtering becomes more effective with increasing displacement

of the receiver line from the source point, as we can see by comparing the unfiltered version of receiver line 3 in Figure 7 with its RT-filtered version in Figure 8. This is important, since surface waves have hyperbolic wavefronts on any receiver line gather which is not collinear with the source point and can be mistaken for reflections. The RT filtering is generally least effective at the apex of a surface wave event, so some residual of the noise may survive at the nearest offset traces in a receiver line gather. We illustrate this in Figures 9 and 10, where we compare the unfiltered and filtered versions of receiver line 8. We note that in Figure 10, most of the coherent energy in the limbs of the surface wave train has been attenuated, while a fairly strong remnant of the apex survives at the centre of the gather at about 1400ms.

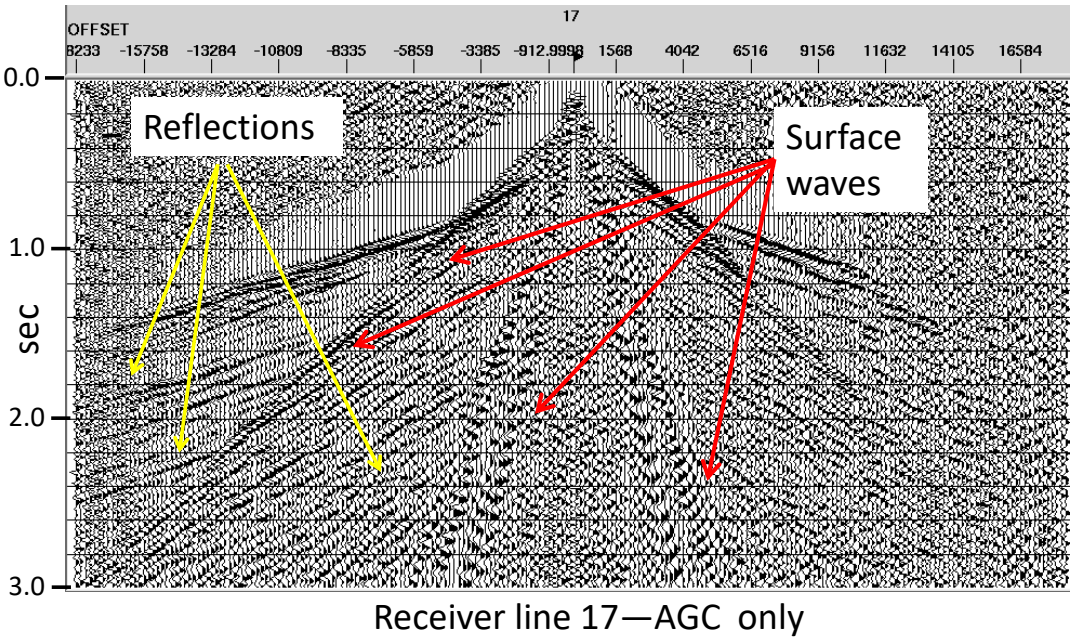

FIG. 5. Receiver line 17 from the centre of our test source gather. This receiver line is collinear with the source point. Very strong surface waves dominate this trace ensemble. These must be attenuated as much as possible to allow interferometry to work properly. The moveout of the surface waves is linear with offset, so always appears linear on a receiver gather collinear with source point.

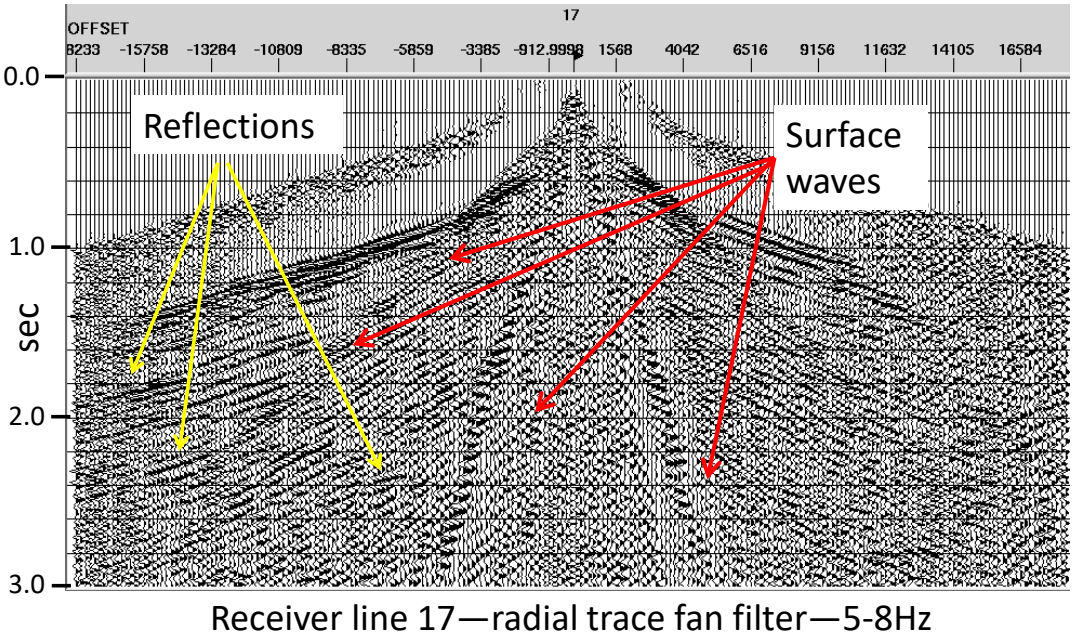

FIG. 6. Receiver line 17 after application of RT filtering to attenuate surface waves. In comparison with Figure 5, noise is significantly diminished, and reflections much stronger. Fragmentary reflections are even present within the cone of residual surface wave noise.

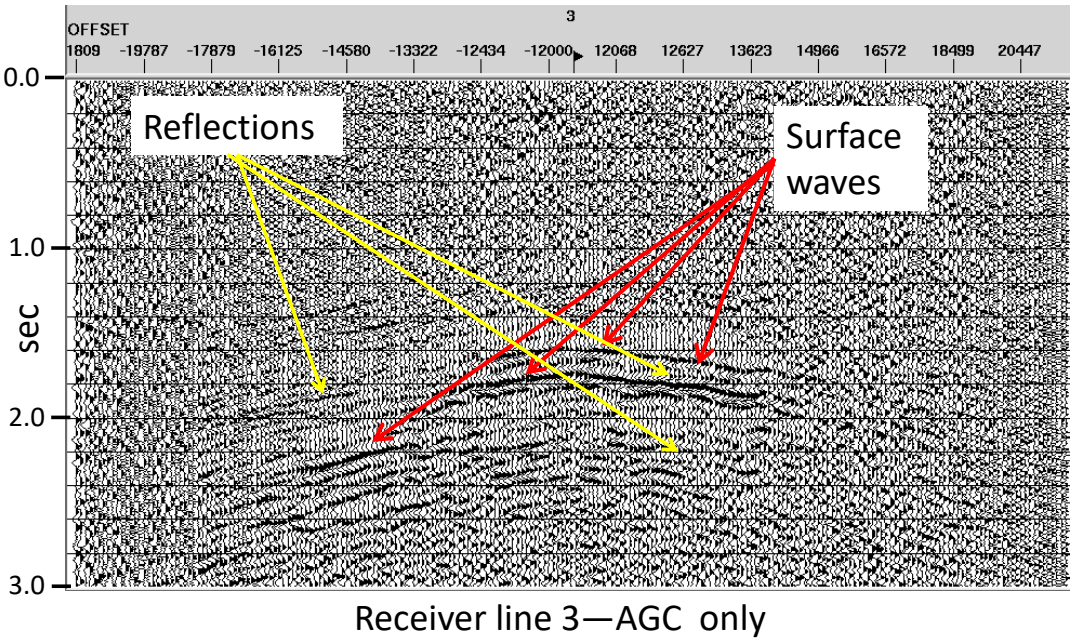

FIG. 7. Receiver line 3, at near maximum lateral displacement from the source point. The projection of the surface waves onto this ensemble makes their moveout hyperbolic instead of linear.

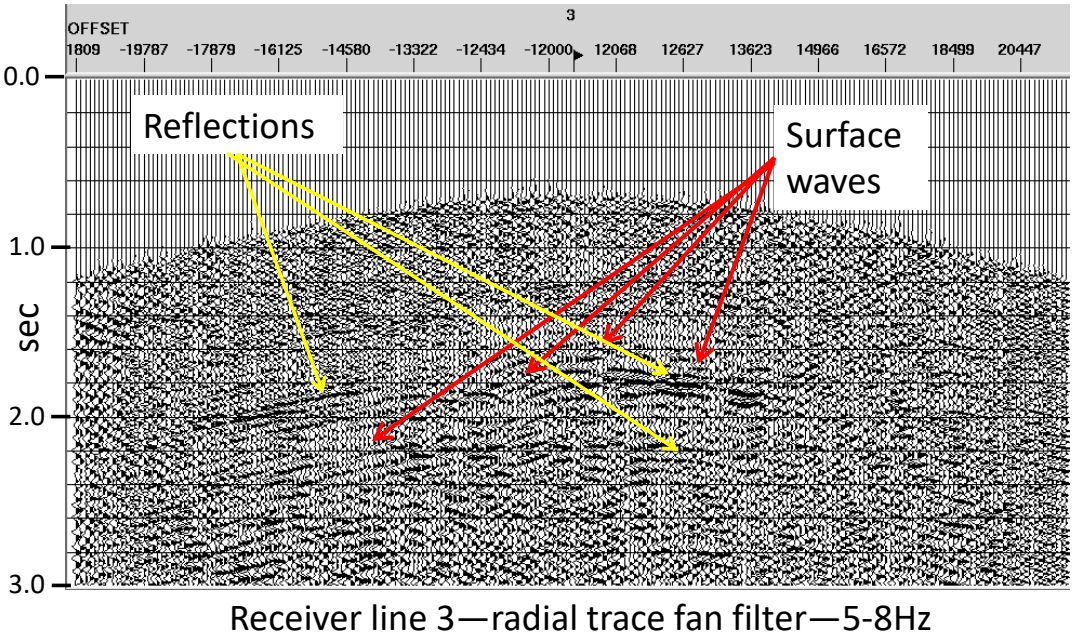

FIG. 8. Receiver line 3 after RT filtering. The effectiveness of the filter is greater at this displacement of the source.

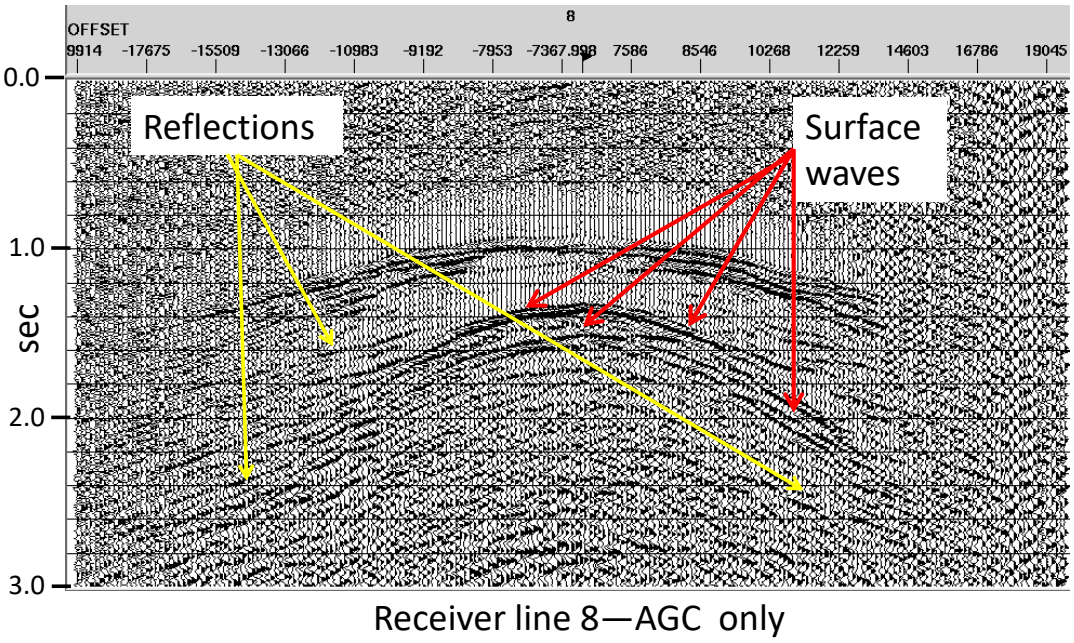

FIG. 9. Receiver line 8, at an intermediate lateral displacement from the source point. Surface waves are hyperbolic in moveout.

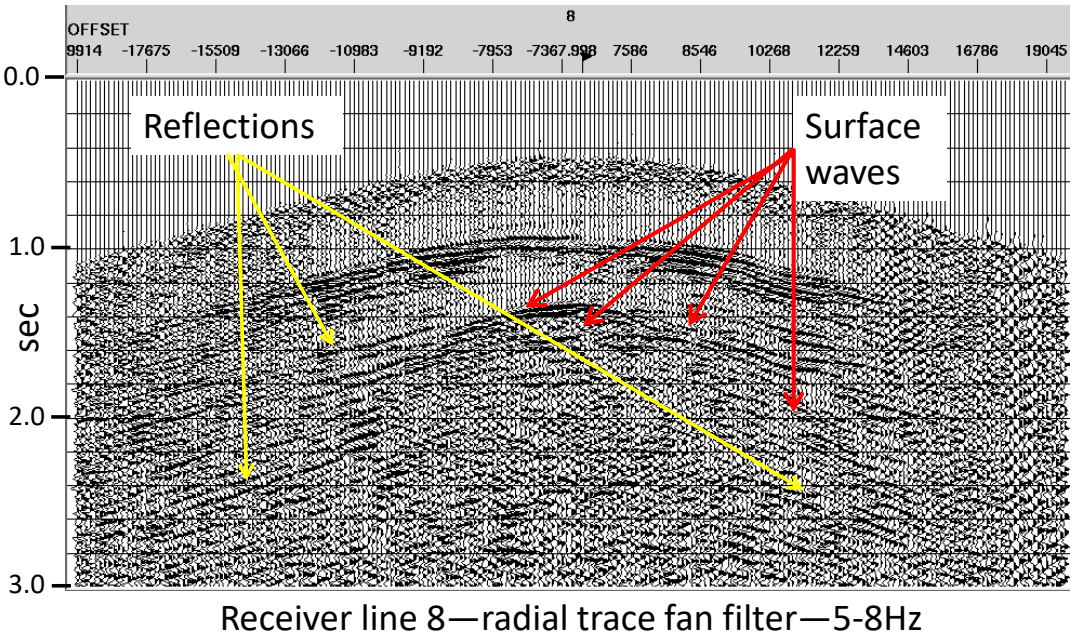

FIG. 10. Receiver line 8 after RT filtering. Filter is most effective at large offsets, least effective at offsets near the apex of the hyperbolic moveout, although even here, the surface wave amplitude is greatly diminished.

The key step in applying the type of interferometry portrayed in Figure 4 is to create an estimated wavefield, against which to cross-correlate the raw data traces. We expect an undisturbed wavefield to be smooth and only slowly varying laterally, essentially a plane wave impinging on the earth's surface and reflecting, unperturbed, from layer boundaries beneath. The way in which we estimate this is by averaging over a large number of traces in an ensemble, assuming that the disturbances caused by the passage of the wavefront through the near surface will average out. Since the shape of the source wavelet is a part of the wavefield, the best estimate of wavelet shape will result when the individual traces being averaged for any given point in the estimated wavefield are as closely aligned as possible before the average. To pursue this alignment, we sometimes resort to applying linear moveout correction, normal moveout correction, or even trim statics, when appropriate, to the raw data traces before averaging them. These are admittedly brute force techniques, but they can result in cleaner, more uniform estimates of the wavefield, which in turn yield more reliable cross-correlations with the raw traces.

Interferometry on receiver line gathers (2D)

- Apply linear moveout correction (LMO) to each receiver line gather to approximately flatten reflections without stretch.
- Apply AGC to receiver line gathers to level trace amplitudes.
- Create estimated wavefield.
    - Apply trim statics procedure within a window to force events within the window to align, for each receiver line gather independently.
    - Apply wide-aperture trace mixing (running average) to each receiver line gather after trim statics—this is the estimated wavefield (2D).
- Match corresponding traces between the LMO-corrected raw trace gathers and the estimated wavefield gathers and cross-correlate.
- Whiten cross-correlations and apply window weights (Henley, 2012a) to form match filters.
- Apply match filters to corresponding raw traces to apply near-surface corrections.
- Compare corrected receiver line gathers with original LMO corrected receiver line gathers.

Interferometry on common-azimuth gathers (3D)

- Apply normal moveout correction (NMO) to each receiver line gather to approximately flatten reflections—use single approximate NMO velocity.
- Apply AGC to level trace amplitudes.

- Remove NMO from receiver line gathers.
- Sort and bin the traces by azimuth and receiver line.
- Create estimated wavefield.
    - Apply LMO.
    - Within each common-azimuth bin, apply wide-aperture trace mixing over receiver line.
    - Sort and bin the traces by receiver line and azimuth.
    - Within each receiver line bin, apply wide-aperture trace mixing over azimuth.
    - Remove LMO.
    - Sort and bin the traces back to azimuth/receiver line bins—this is the estimated wavefield (3D).
- Match corresponding traces between the raw azimuth/receiver line bins and the estimated wavefield bins and cross-correlate.
- Condition the cross-correlations to form match filters.
- Apply match filters to corresponding raw azimuth/receiver line bin traces to apply near-surface corrections.
- Sort to receiver line gathers.
- Compare corrected receiver line gathers with original receiver line gathers.

Interferometry on common-raypath gathers (3D)

- Apply normal moveout correction (NMO) to each receiver line gather to approximately flatten reflections—use single approximate NMO velocity.
- Apply AGC to level trace amplitudes.
- Remove NMO from receiver line gathers.
- Sort and bin the traces by azimuth and offset.
- Create estimated wavefield.
    - Apply LMO.

  - Within each common-azimuth bin, apply wide-aperture trace mixing over offset.
  - Sort and bin the traces by offset and azimuth.
  - Within each common-offset bin, apply wide-aperture trace mixing over azimuth.
  - Remove LMO.
  - Sort and bin the traces back to azimuth/offset bins—this is the estimated wavefield.

- Apply interferometry in the common-raypath domain.
  - Apply Tau-P transform to azimuth/offset sorted raw data—each common-azimuth ensemble yields one Tau-P transform.
  - Apply Tau-P transform to azimuth/offset sorted estimated wavefield—each ensemble yields one Tau-P transform.
  - Match corresponding Tau-P traces between the raw data Tau-P ensembles and the estimated wavefield Tau-P ensembles and cross-correlate.
  - Condition the cross-correlations to create match filters.
  - Apply the match filters to corresponding Tau-P traces of the raw data Tau-P ensembles to apply near-surface corrections in the raypath direction.
  - Apply inverse Tau-P transform to corrected Tau-P ensembles to recover azimuth/offset bins of X/T traces.

- Sort corrected traces to receiver line gathers.
- Compare corrected receiver line gathers with original receiver line gathers.

RESULTS

To present the results of our interferometry experiments, we always display the data from our 3D source gather in the form of receiver line gathers, since those provide the best-sampled views of reflections, including trace-to-trace variations that may be indicative of near-surface effects. Since there are 32 receiver line gathers in our experimental source gather, we choose to display only gathers that we feel are ‘representative’, in the sense that they range in displacement from the source point from far to one side of the source point, to mid-range, to near coincidence, to mid-range and far on the other side of the source point. We use these same receiver lines to demonstrate the results for each of our interferometry variations.

2D interferometry on receiver lines

Figure 11 shows RT-filtered receiver line 3 after application of LMO correction, and Figure 12 shows the result of the 2D interferometric technique applied to the receiver line gather as described above. As can be seen, reflection coherence has increased significantly at all levels. The window used for the interferometry was broad enough to include all significant reflections.

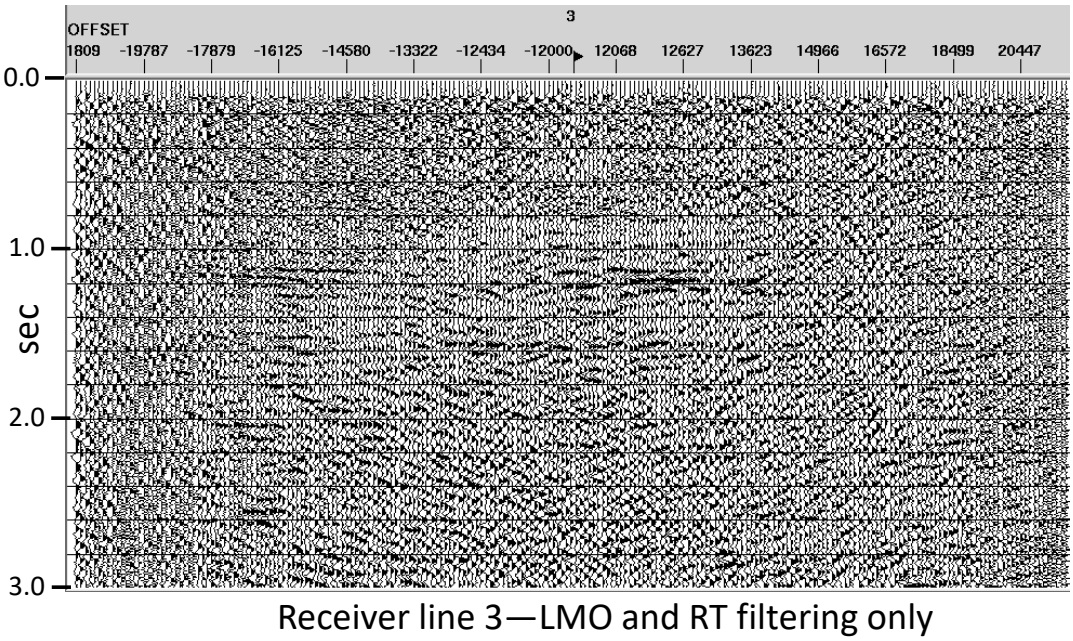

FIG. 11. Receiver line 3, with Linear moveout removed, after RT filtering.

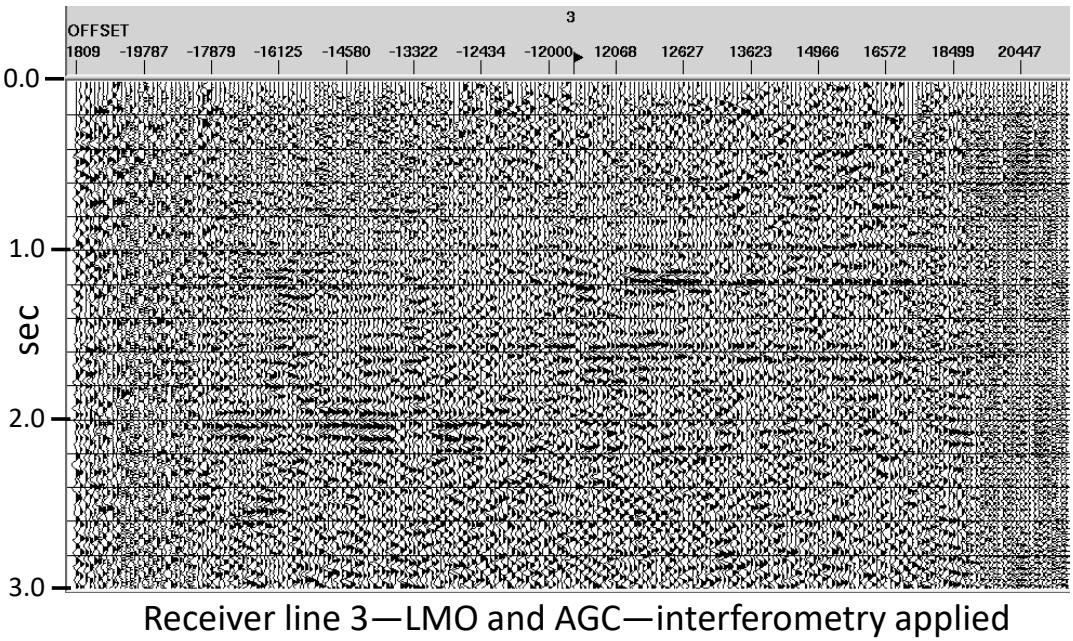

FIG. 12. Receiver line 3 after application of 2D interferometry to improve coherence of reflections along receiver line. For broadside reflections like these, LMO is a good approximation to NMO, and has the advantage that traces are not stretched, as they would be with NMO correction.

When we move to receiver line 8, we encounter problems due to the remnant of the surface wave not attenuated by RT filtering. Figure 13 shows the RT-filtered receiver line gather after LMO correction. When we apply 2D interferometry over a window which includes reflections as well as nearly horizontal coherent segments of residual noise, the result is shown in Figure 14. Note that reflection coherence is generally increased at all levels, except in the vicinity of the interfering noise remnant, where the shallowest reflections are less coherent. Interestingly, however, deeper reflections at about 2000ms are more coherent. If we apply the interferometry over a narrow window which does not include the noise remnant, we can indeed align shallow reflections, as in Figure 15, but the deeper reflections are then not properly corrected. This may indicate that required corrections are non-stationary and may require a raypath-consistent approach.

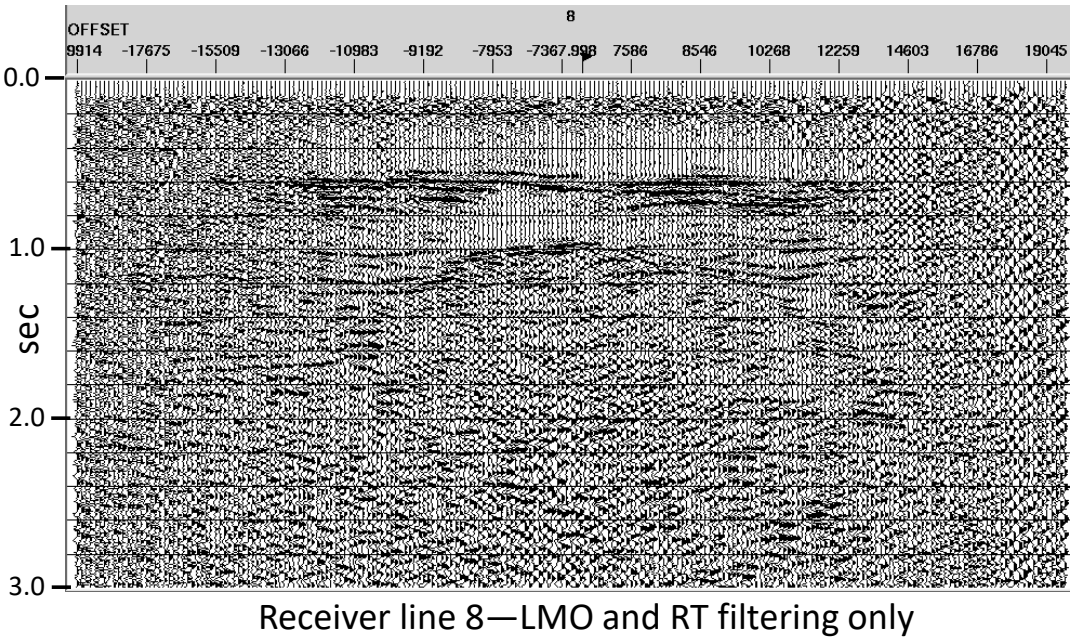

FIG. 13. Receiver line 8 after being RT filtered and having LMO removed. LMO is still a good approximation for NMO, even at these shorter offset distances. Residual coherent noise is nearly parallel to apparent reflections.

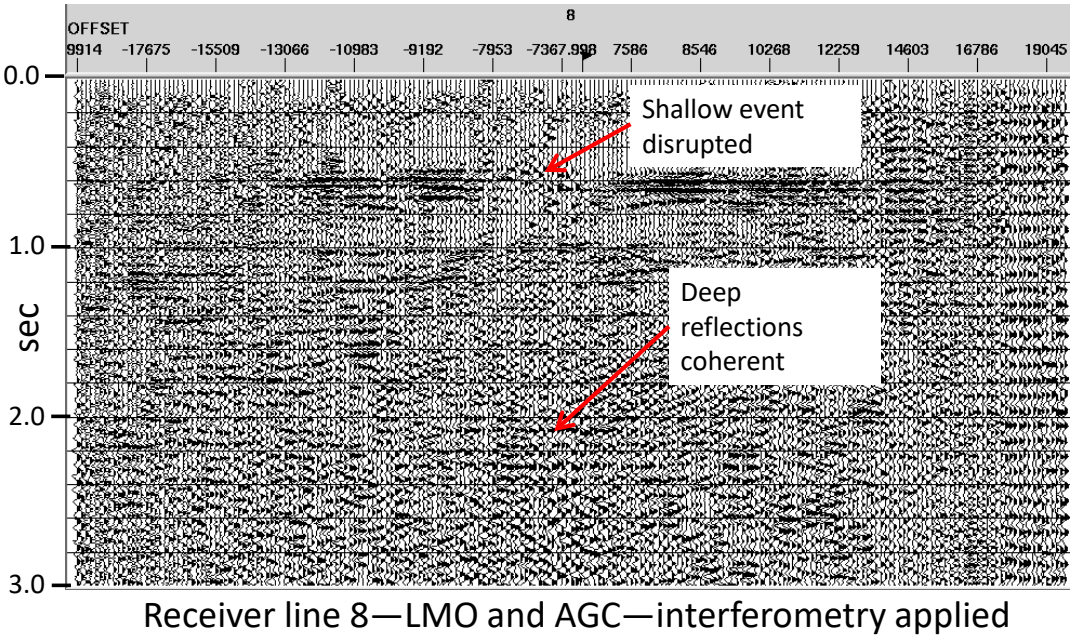

FIG. 14. Receiver line 8 after 2D interferometry to improve coherence of reflections along receiver line. Because the interferometry is affected by the remnant of coherent noise, shallower events are misaligned in the vicinity of the strongest residual noise.

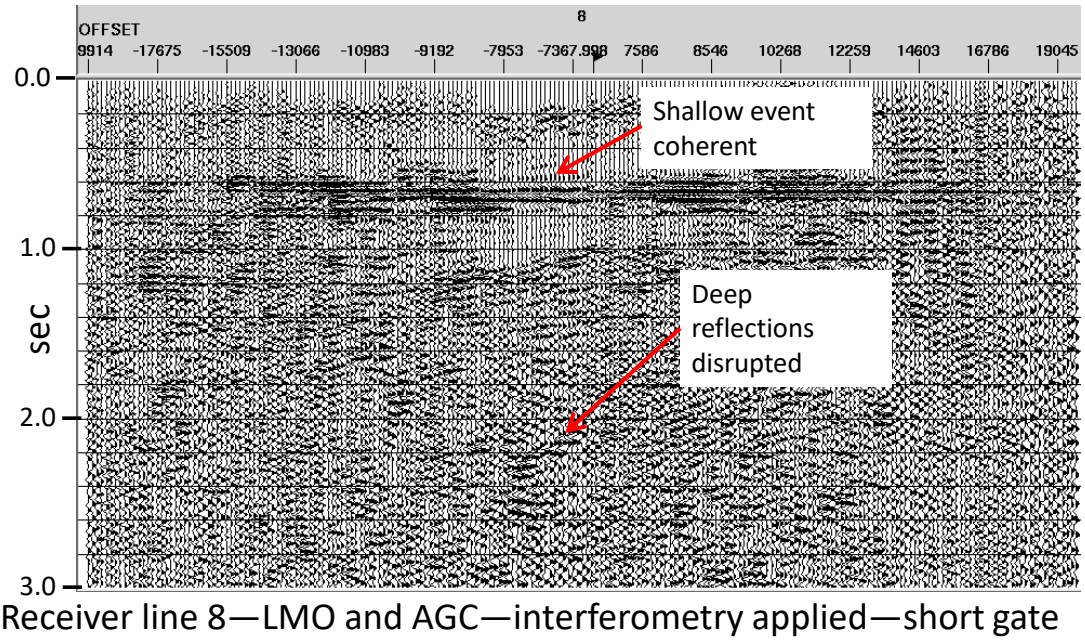

FIG. 15. If a short, shallow window is used to apply 2D interferometry, the noise can be excluded from the process, making shallow events more coherent...but deep reflections then suffer.

When the remnant noise is coherent but not parallel to reflections, as in receiver line 17, shown in Figure 16, the interferometry can be relatively successful, as shown in Figure 17. When the interfering noise remnant lies on top of significant reflections, but is not coherent, as on receiver line 21, shown in Figure 18, the 2D interferometry may be moderately successful, as in Figure 19. On another receiver line with significant displacement from the source point, receiver line 30, in Figure 20, we find once again that 2D interferometry is quite successful (Figure 21), probably because most coherent noise has been attenuated..

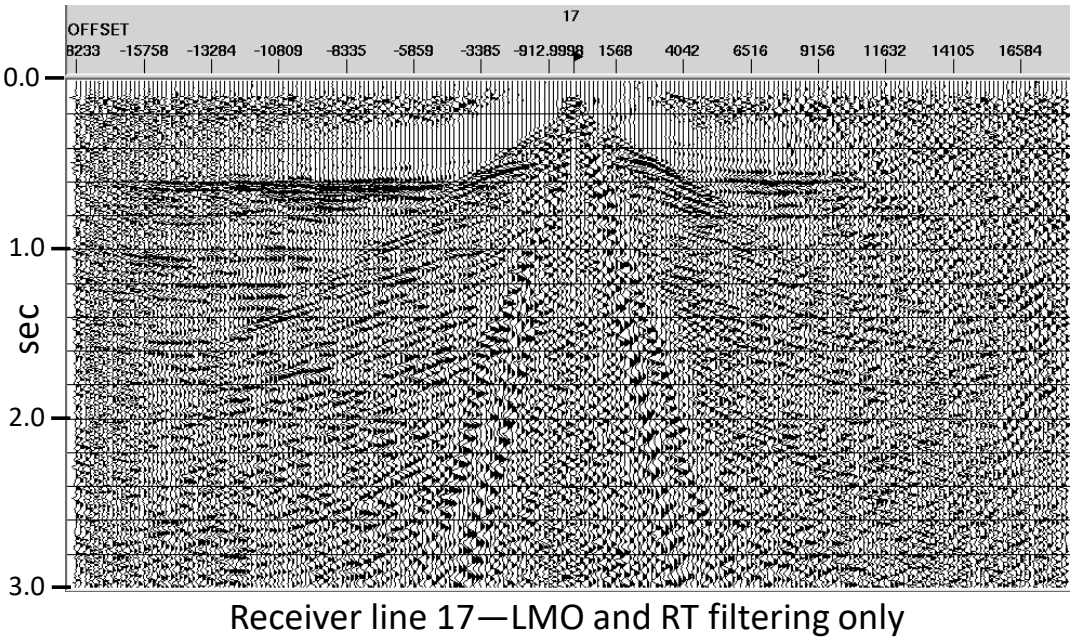

FIG. 16. Receiver line 17 after RT filtering and LMO. Coherent noise remnants here do not nearly align with reflections as on receiver line 8 in Figure 13.

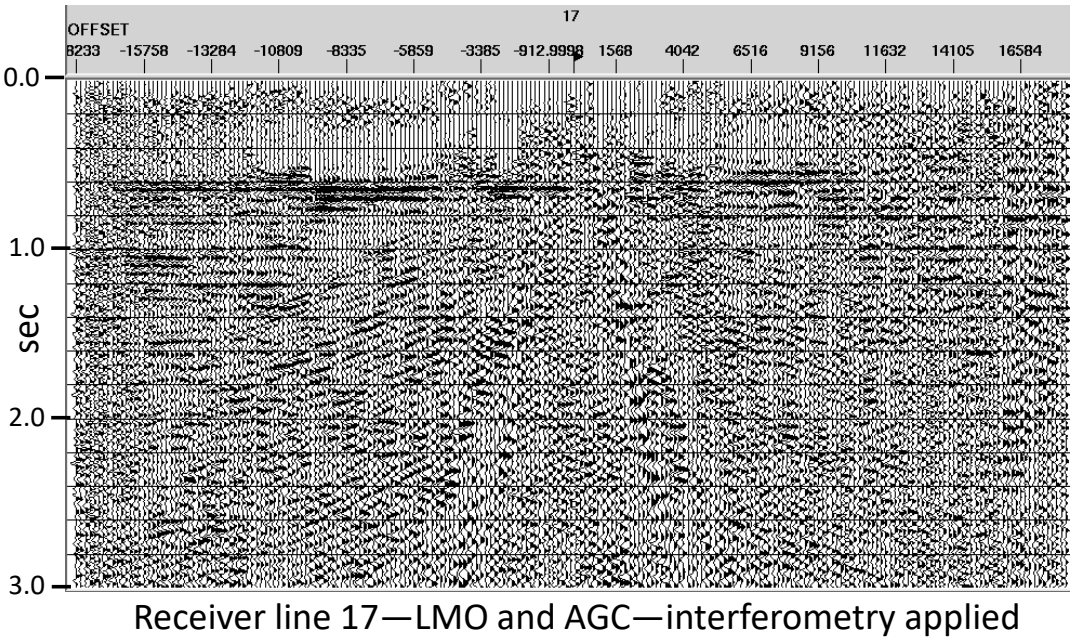

FIG. 17. 2D interferometry applied to receiver line 17 seems not to be greatly affected by residual coherent noise, probably because noise events, although coherent, are oblique to reflections.

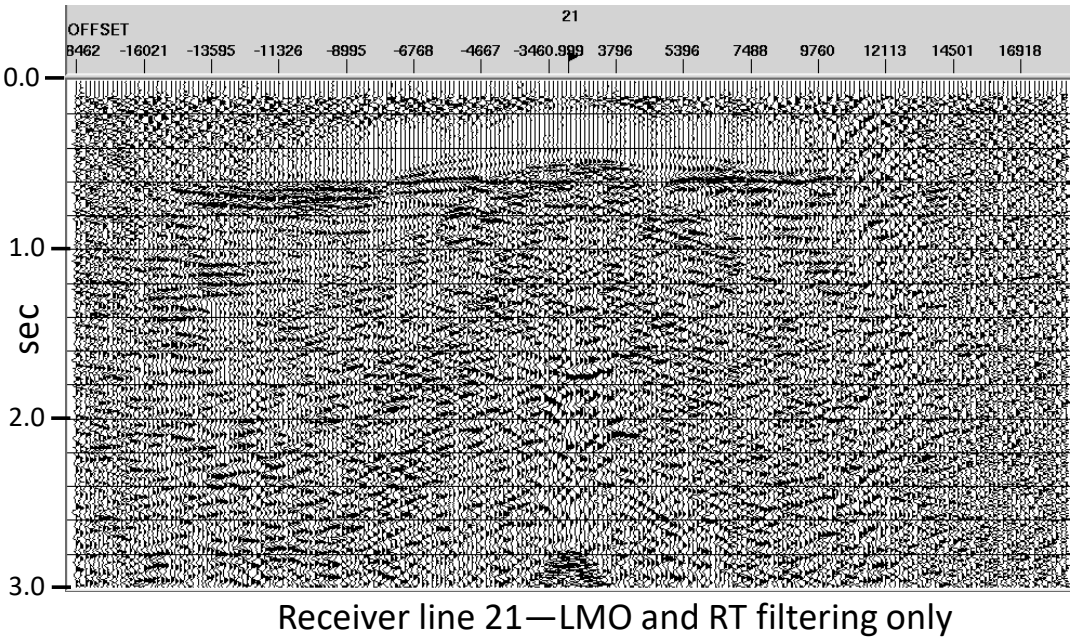

FIG. 18. Receiver line 21 after RT filtering and LMO. Although residual noise is present, much of it is not coherent in a direction parallel to reflections.

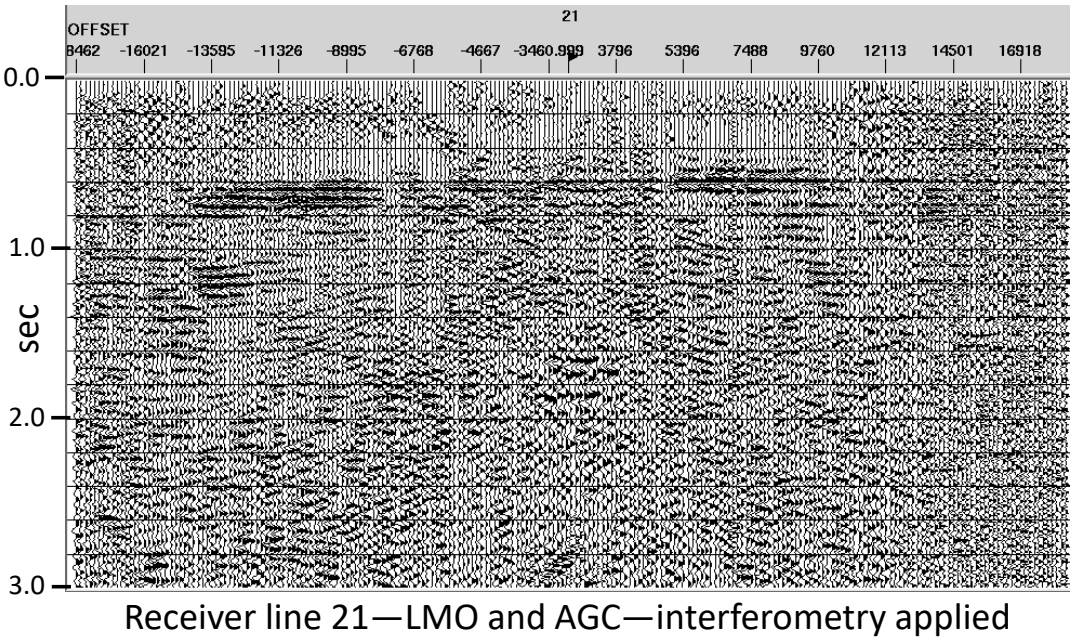

FIG. 19. 2D interferometry applied to receiver line 21. Residual noise has clearly not greatly affected the interferometry...we can see continuous reflections both shallow and deep.

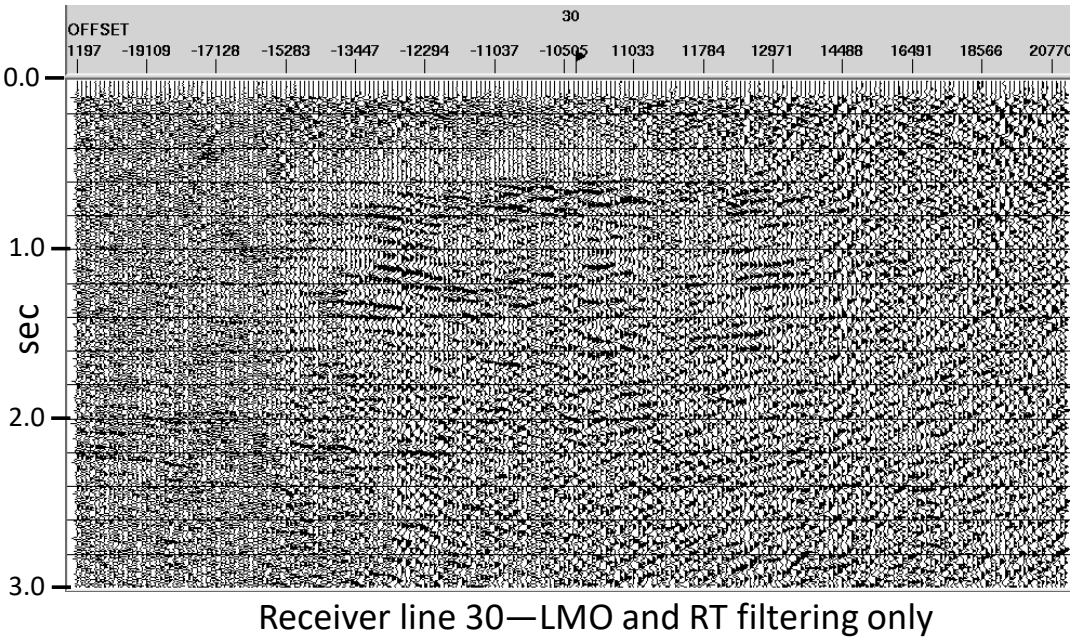

FIG. 20. Receiver line 30 after RT filtering and LMO.

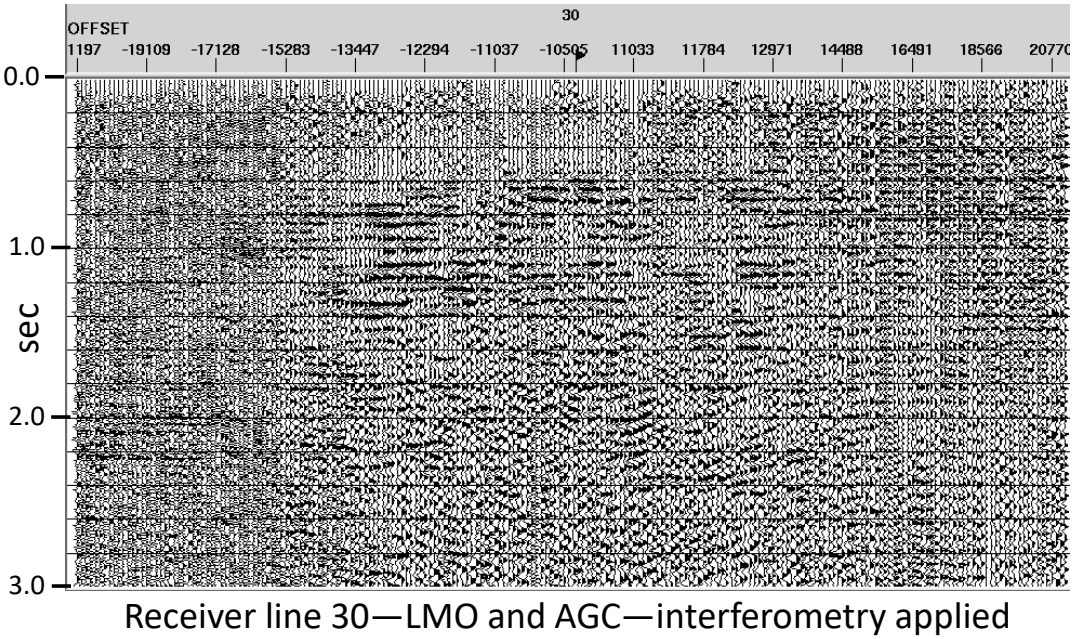

FIG. 21. 2D interferometry applied to receiver line 30. Reflection alignment and coherence much improved.

In summary, 2D interferometry applied to individual receiver line gathers of 3D source ensembles can significantly increase the strength and coherence of reflections, but the result is not uniform for all gathers. Because remnants of coherent noise after application of RT filtering can affect the interferometry process, receiver lines whose displacement from the source point puts them well away from the surface wave cone show the best results. Remnant surface waves can affect the interferometry process in two ways; first by contaminating the trace mixing applied to the receiver line gather to obtain the estimated wavefield, and second by contaminating legitimate reflection events being correlated with the estimated wavefield. This interferometry process can tolerate residual noise only if it is either incoherent, or non-parallel.

Furthermore, since there is no attempt to reconcile the corrected receiver line gathers with each other, this is truly a 2D process and may be of limited use—perhaps as more of a diagnostic tool than an actual processing technique.

3D interferometry on common-azimuth gathers

To prepare the RT-filtered receiver line ensembles for processing in the azimuth and receiver line or offset domains, we created 36 common azimuth bins, each 10 degrees wide, into which to sort the data. Because of the way that radially distributed azimuth bins intersect the receiver lines, the distribution of traces within each bin varied considerably, both in the number of traces and the uniformity of the distribution. We illustrate first with Figure 22, which shows a common azimuth ensemble for azimuth bin number 4, sorted by receiver line within the bin. The same bin sorted by offset appears in Figure 23, where we can see only minor differences in trace order. Either ensemble appears suitable for the application of interferometry correction, because of the relative continuity of reflection events. Figure 24 shows azimuth bin number 17, sorted by receiver line, while Figure 25 shows the same bin sorted by offset. In this case, the sort has mainly served to affect the overall order of the traces in the ensemble—either one appears suitable for interferometry. In the case of azimuth bin number 30, shown in Figure 26, sorted by receiver line, and in Figure 27, sorted by offset, the order of the sort within the bin has significantly affected the continuity and coherence of events across the ensemble, with offset-ordered traces showing far more trace-to-trace coherence. This indicates that for at least some azimuth bins, depending upon their orientation relative to receiver lines, sorting them by offset yields ensembles better suited for interferometry. For what follows, we sorted the common-azimuth ensembles by receiver line for applying interferometry in the X/T domain, and by offset for applying interferometry in the raypath domain.

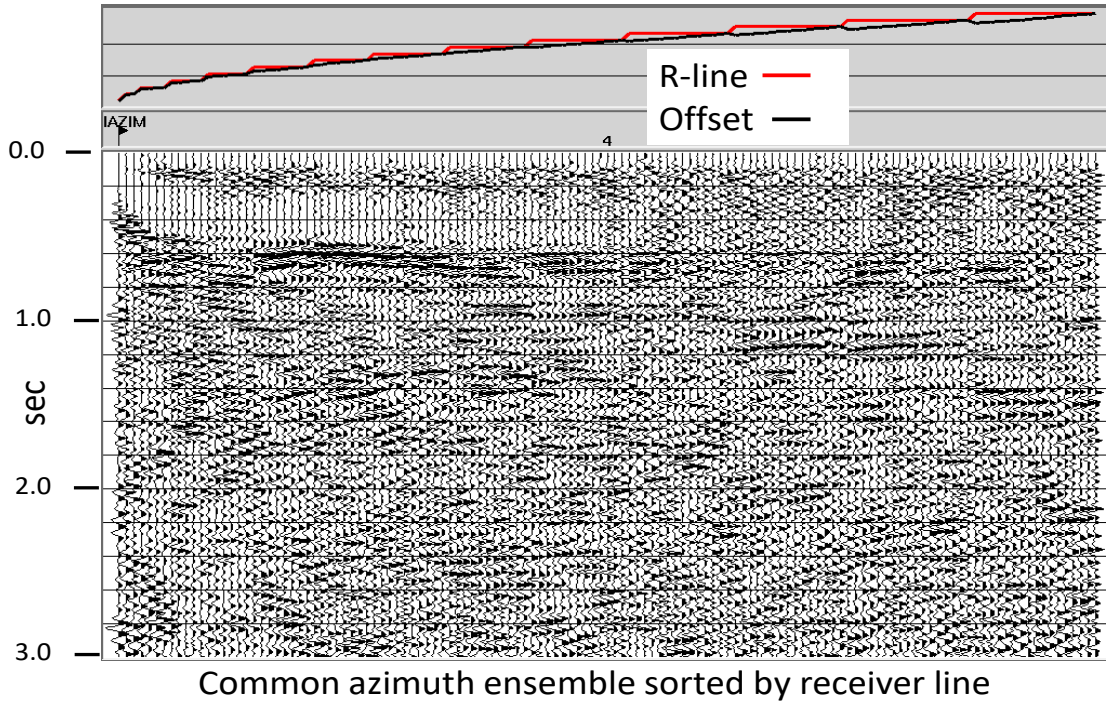

FIG. 22. Common azimuth ensemble for Azimuth bin 4, sorted by receiver line. For this particular azimuth, secondary sort on receiver line is nearly the same as secondary sort on offset.

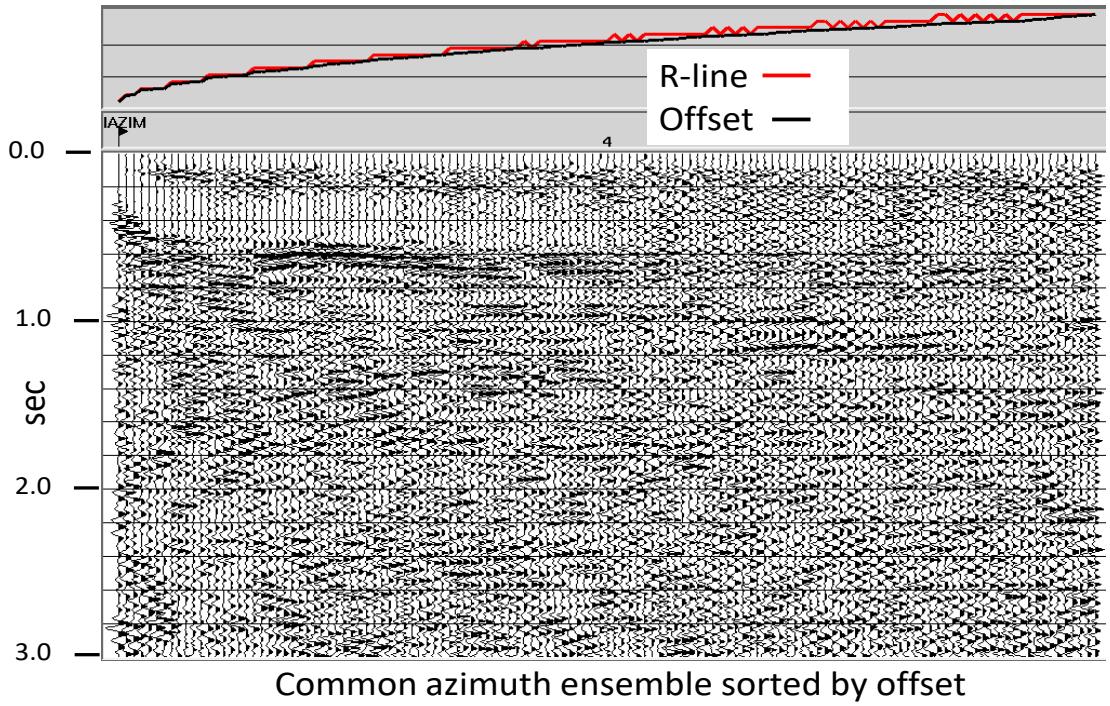

FIG. 23. Common azimuth ensemble 4, with secondary sort on offset. Trace order is not much different from that in Figure 22.

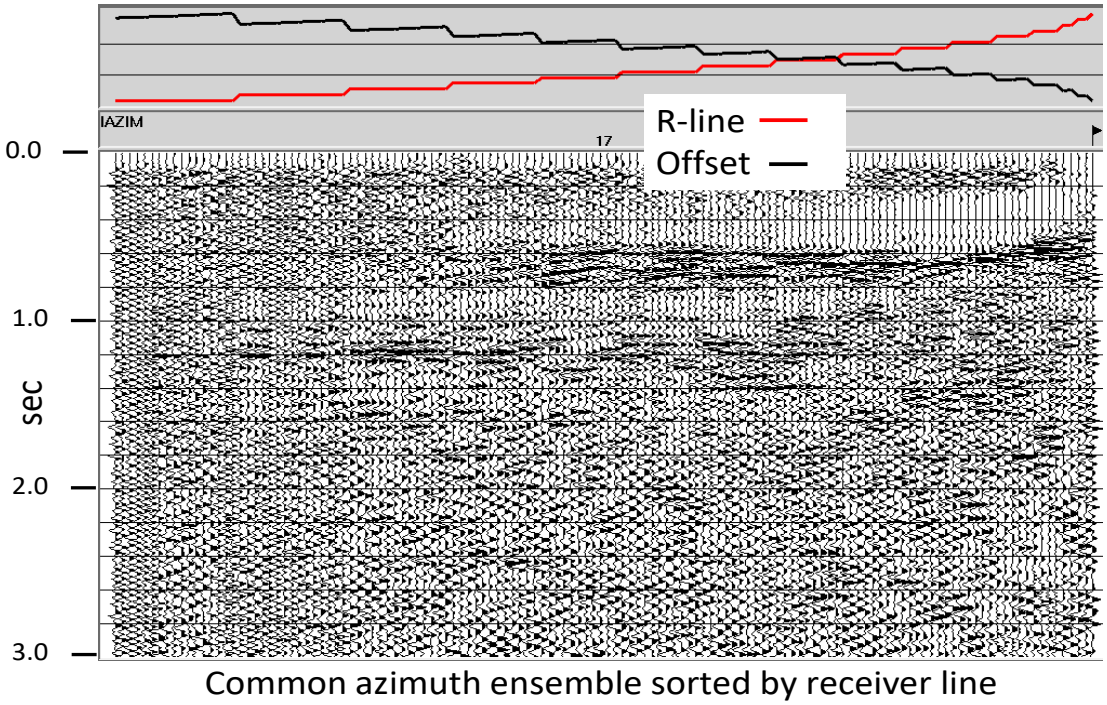

FIG. 24. Common azimuth ensemble 17 with secondary sort on receiver line.

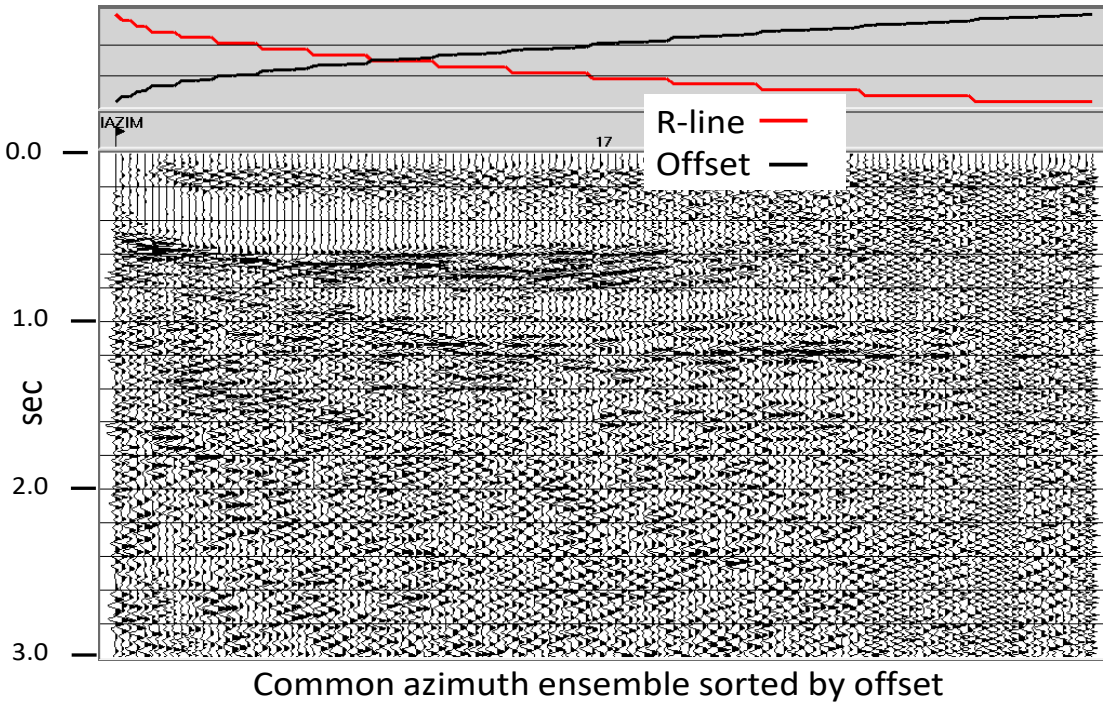

FIG. 25. Common azimuth ensemble 17 with secondary sort on offset. Trace order is approximately reversed from that in Figure 24.

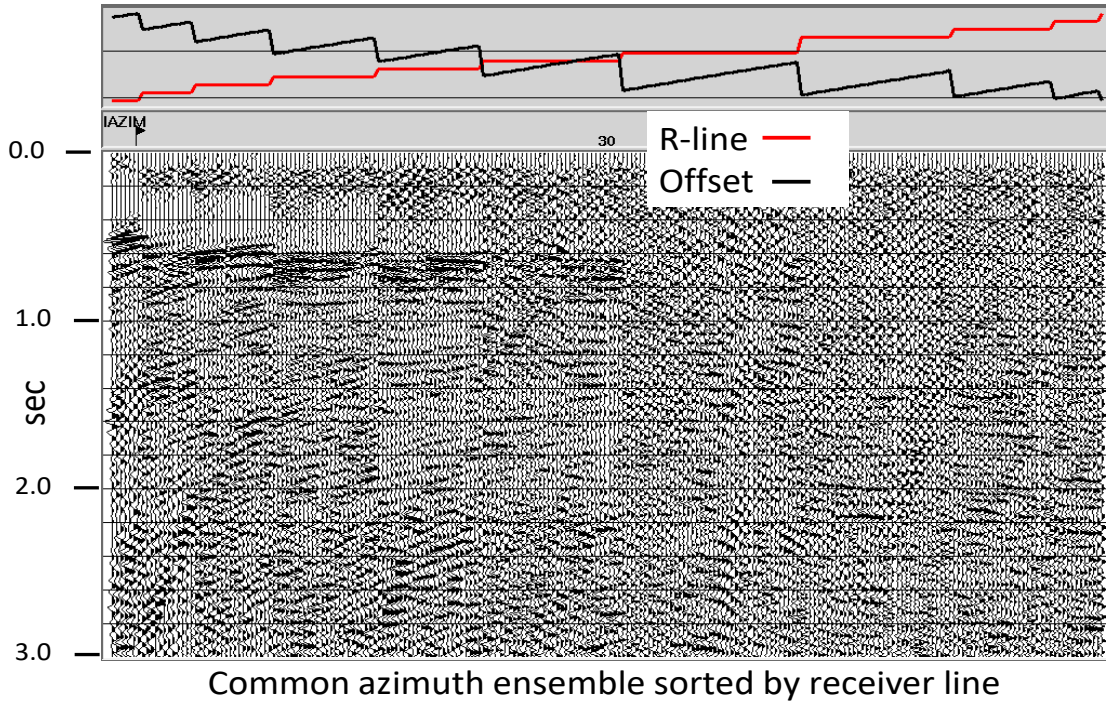

FIG. 26. Common azimuth ensemble 30 with secondary sort on receiver line.

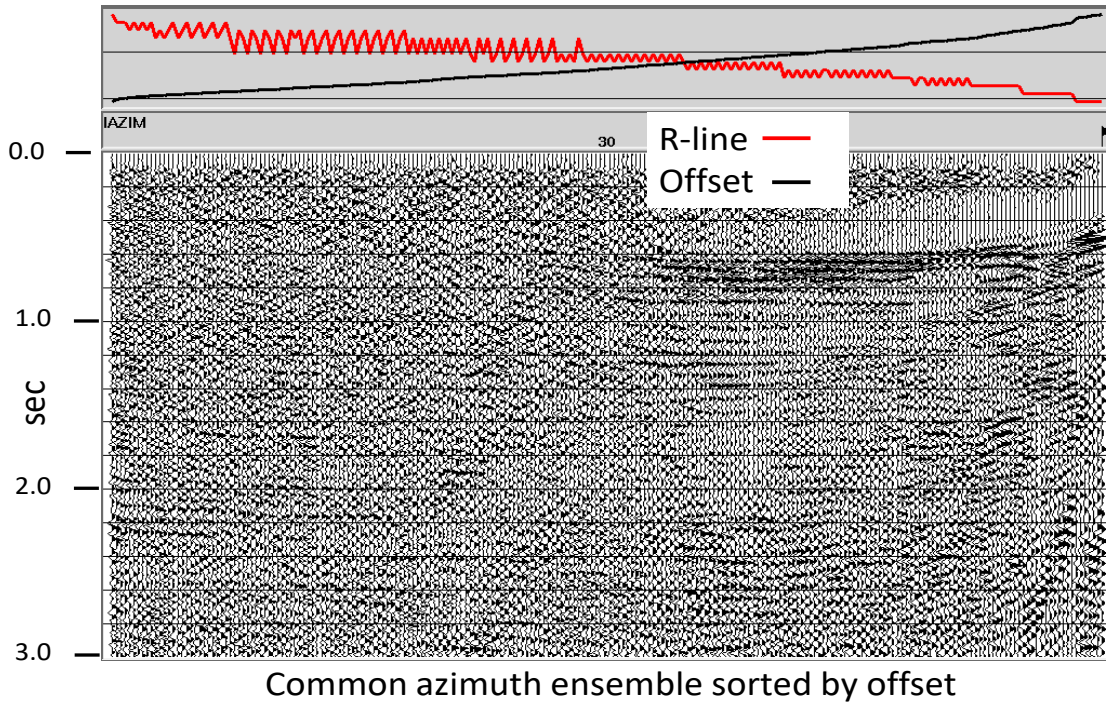

FIG. 27. Common azimuth ensemble 30 with secondary sort on offset. The coherent events are better organized in this ensemble than in Figure 26.

Figure 28 shows receiver line 3 after RT-filtering, and Figure 29 shows the same receiver line after application of 3D interferometry to its constituent azimuth gathers. Significant improvement in reflection coherence is apparent over most of the ensemble. Figures 30 and 31 show the same displays for receiver line 8. While the improvement in coherence of the reflections is not as pronounced as for receiver line 3, it is notable that performing the interferometry in 3D is not particularly affected by the noise remnant, in contrast to the 2D result shown earlier. Likely, this is because the noise residual is not as organized in the azimuth/receiver-line domain as in the receiver-line/offset domain. Receiver line 17 is portrayed in Figures 32 and 33, where we again see a modest reflection coherence improvement from the 3D interferometry that appears not to be affected by the residual coherent noise. Similar results are seen for both receiver lines 21 and 30, displayed in Figures 34 and 35, and Figures 36 and 37, respectively. In each case, 3D interferometry has modestly improved reflection strength and coherence.

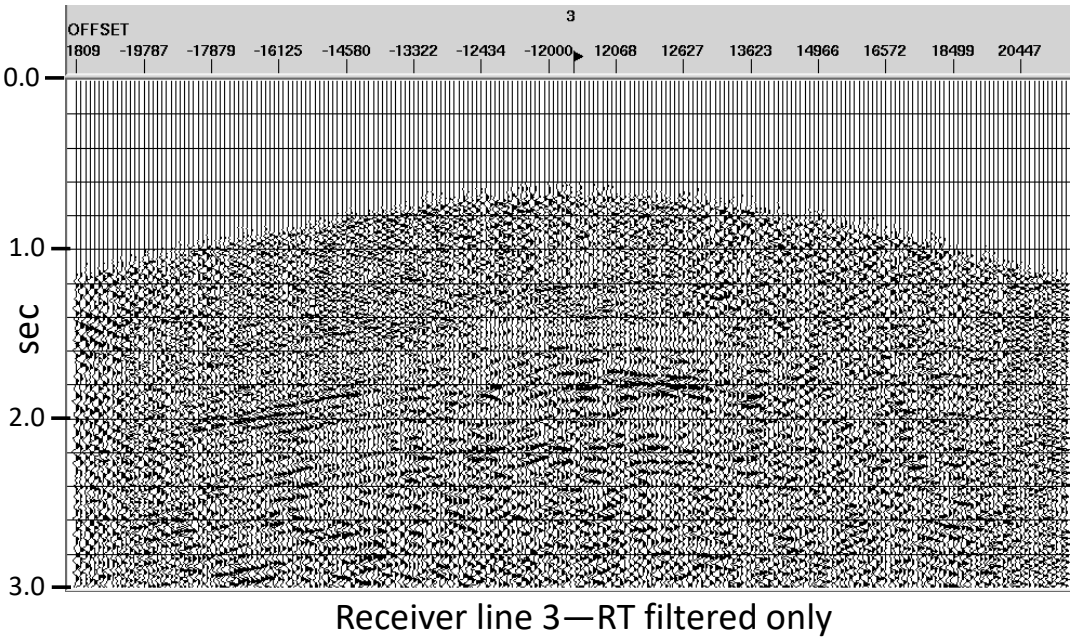

FIG. 28. Receiver line 3 after RT filtering to remove surface waves.

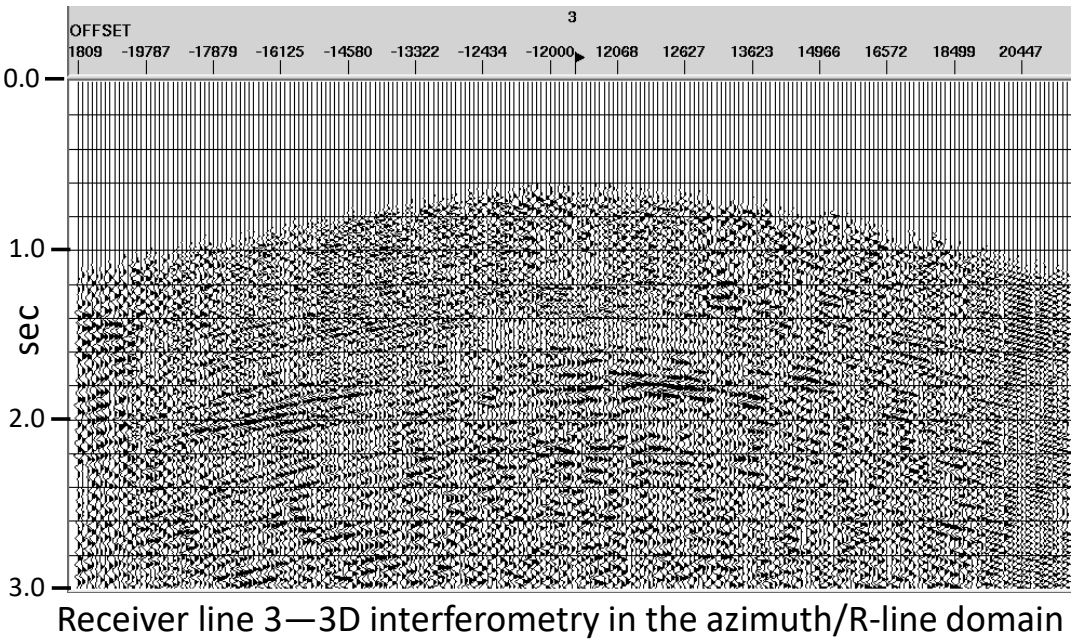

FIG. 29. Receiver line 3 after 3D interferometry applied to the azimuth/receiver line trace ensembles. Event coherence and continuity have increased at all levels.

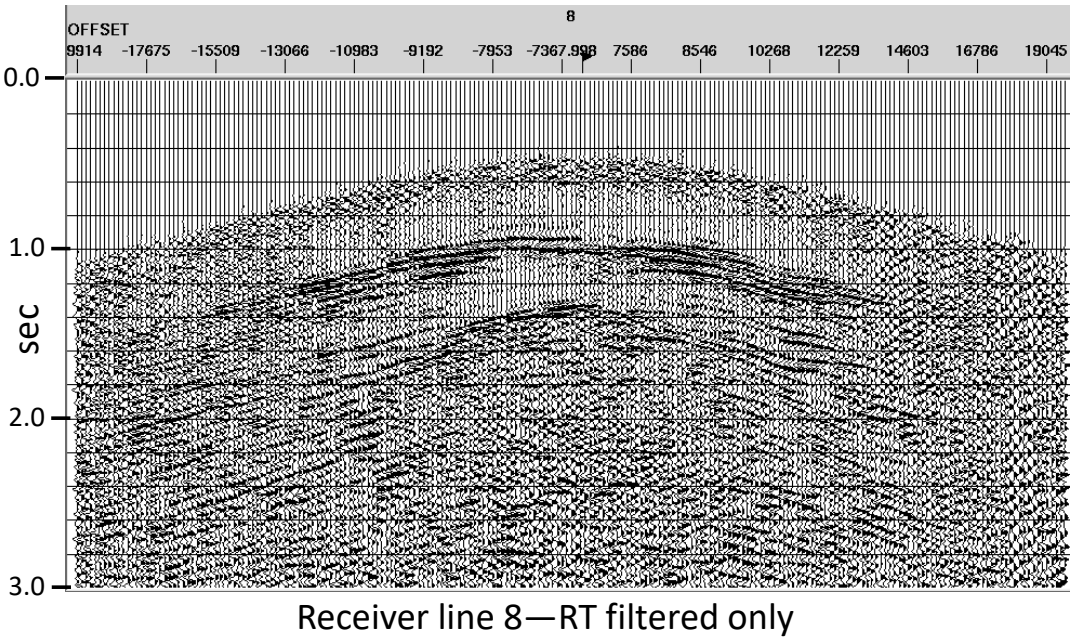

FIG. 30. Receiver line 8 after RT filtering to remove surface waves.

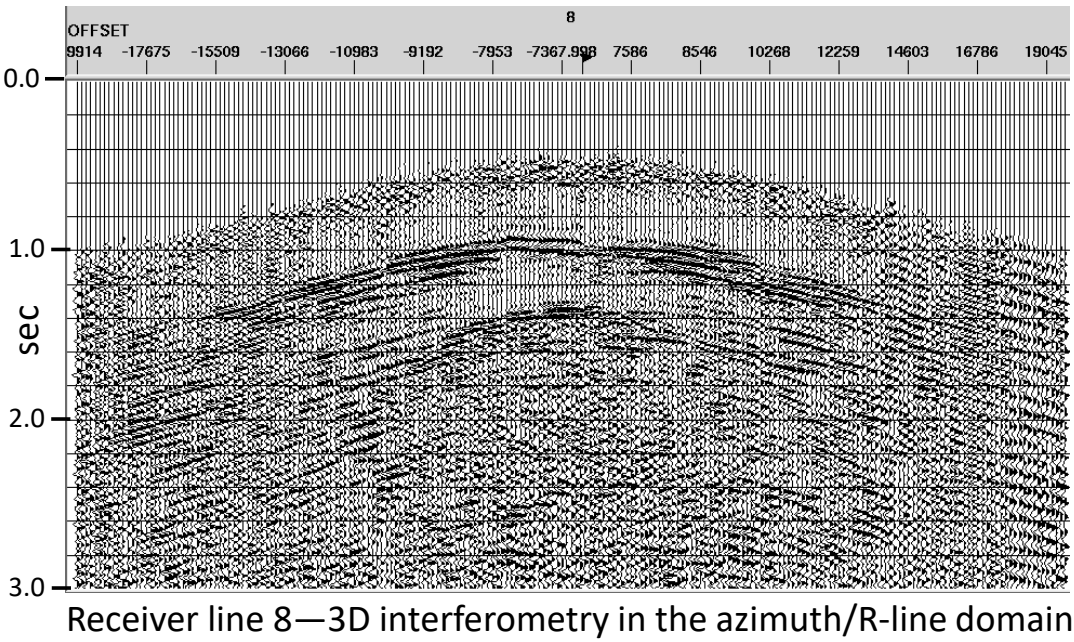

FIG. 31. Receiver line 8 after 3D interferometry applied to the azimuth/receiver line ensembles. Event coherence mostly improved, but affected by residual surface wave noise.

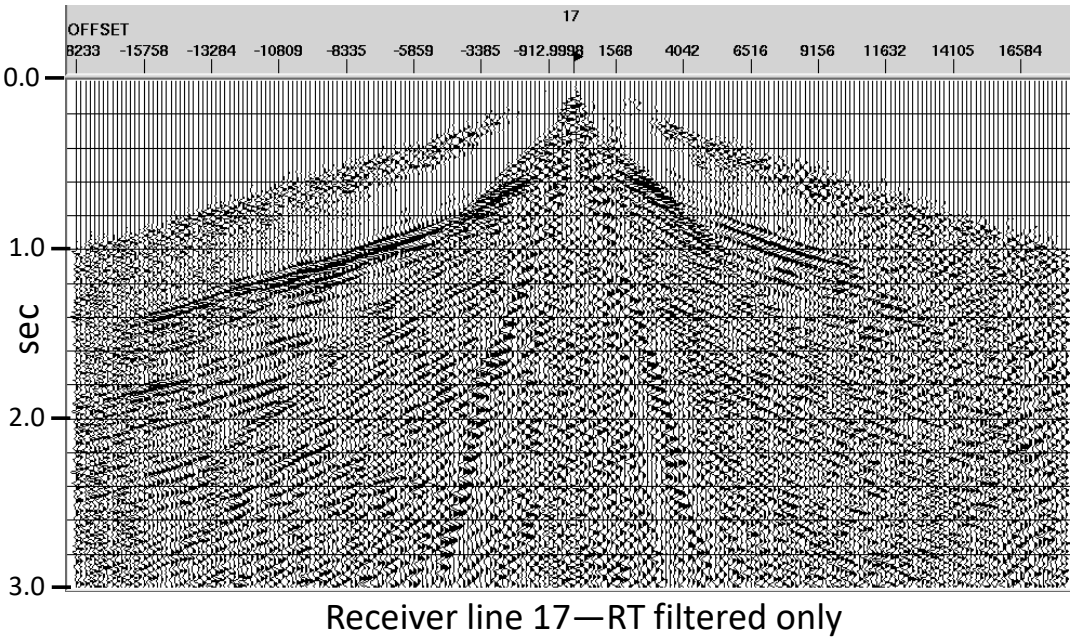

FIG. 32. Receiver l;ine 17 after RT filtering to remove surface waves.

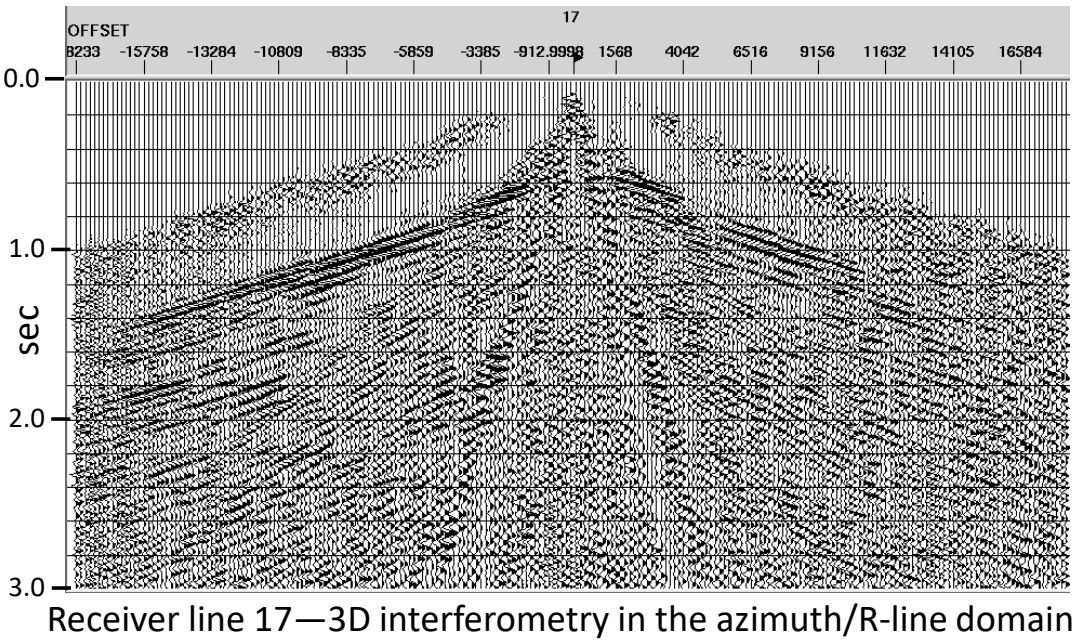

FIG. 33. Receiver line 17 after 3D interferometry applied to the azimuth/receiver line ensembles. Moderate improvement in reflection event coherence.

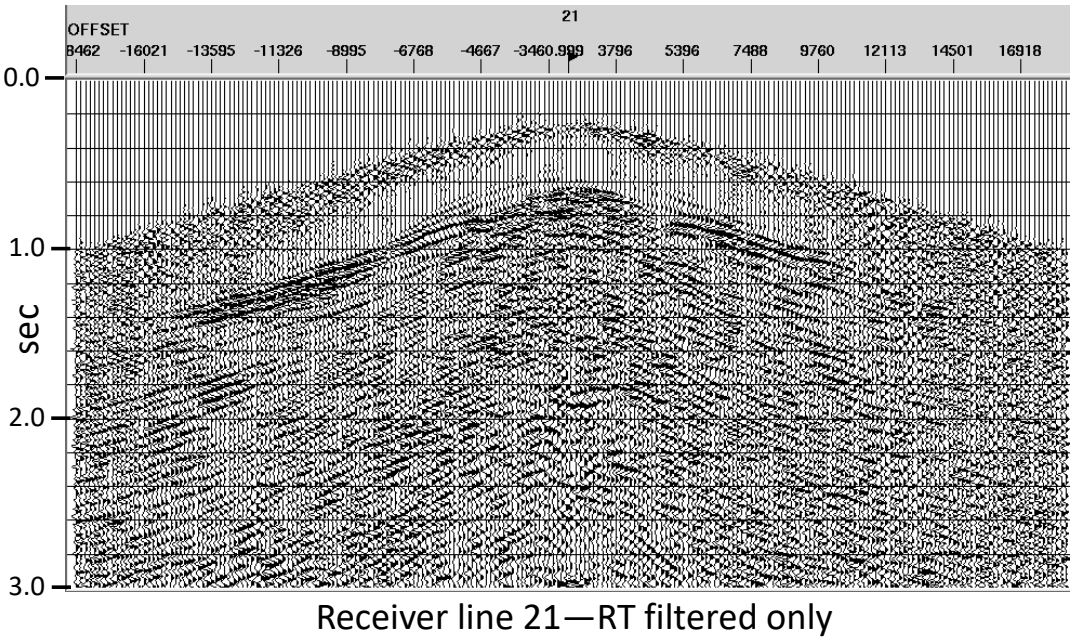

FIG. 34. Receiver line 21 after RT filtering to remove surface waves.

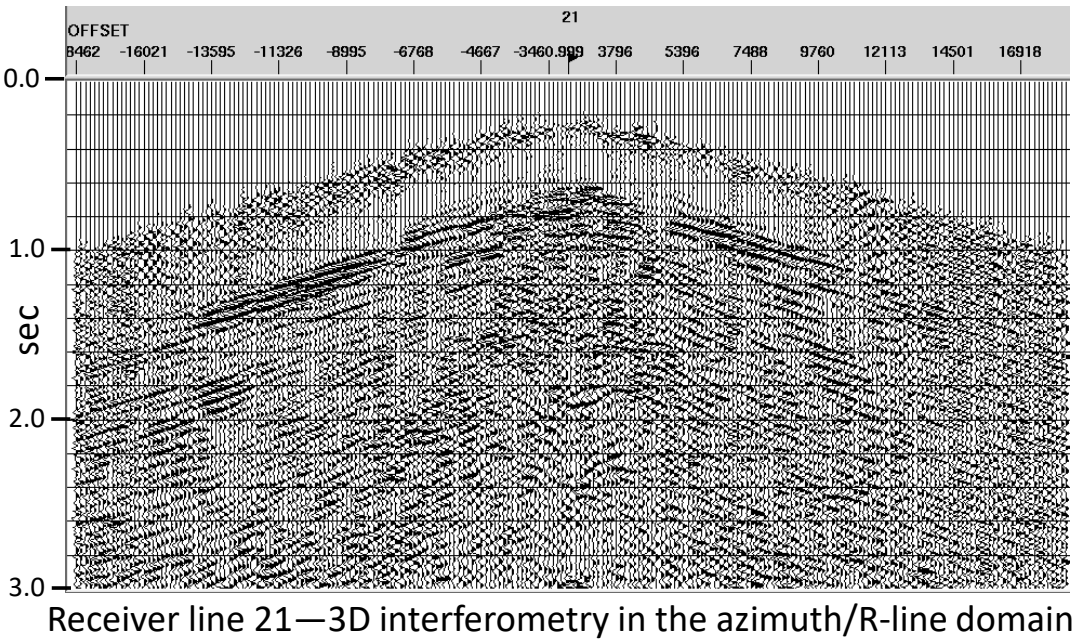

FIG. 35. Receiver line 21 after 3D interferometry applied to the azimuth/receiver line ensembles. Modest improvement in coherence of reflections.

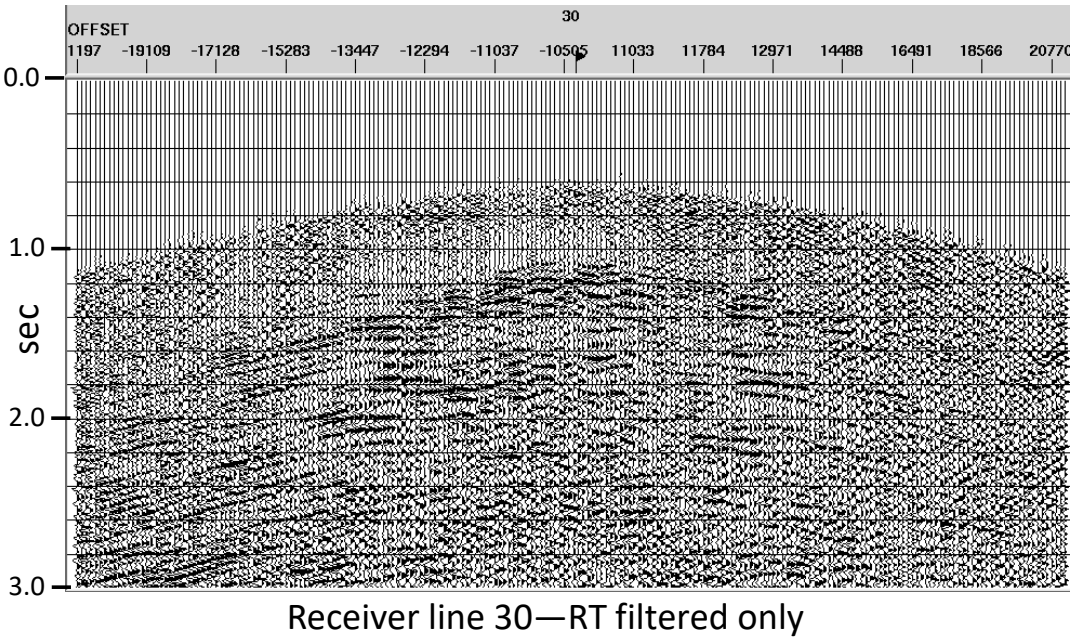

FIG. 36. Receiver line 30 after RT filtering to remove surface waves.

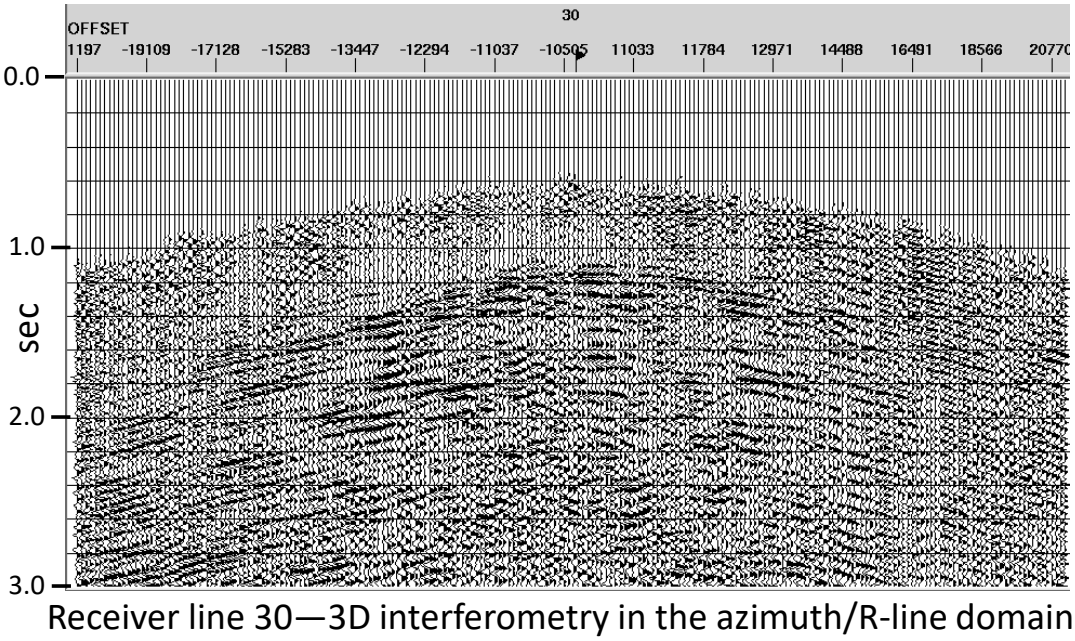

FIG. 37. Receiver line 30 after 3D interferometry applied to azimuth/receiver line ensembles. Significant improvement in reflection event continuity and coherence.

To summarize, 3D interferometry in the X/T domain appears to offer significant improvement in reflection strength and continuity, and seems not to be affected by residual coherent noise. This is likely due to the fact that noise is less organized in the azimuth/receiver-line or azimuth/offset domains than in the receiver-line/offset domain. The biggest improvement was seen in the receiver lines with the most displacement from the source point, where the traces have the largest offset. While 2D interferometry on receiver lines appears to improve coherence more, this may be a slightly deceptive result, since the interferometry does not correlate between receiver lines themselves. In 3D, on the other hand, the estimated wavefield is 3D, so that corrections derived and applied to traces in common-azimuth ensembles help tie the receiver lines together in a 3D sense.

3D interferometry in the raypath domain

All interferometry shown to this point has been applied to X/T domain traces, assuming that near-surface corrections are stationary. As a further test, we transformed azimuth/offset ensembles, and their corresponding estimated wavefield ensembles to the Tau-P domain, where each P trace corresponds to a different raypath angle. We then cross-correlated corresponding P traces, conditioned the cross-correlations, and applied the conditioned functions as match filters to the P traces of the azimuth/offset ensembles. The inverse Tau-P transforms then yielded corrected azimuth/offset ensembles in the X/T domain, which were then re-sorted to receiver lines for comparison to earlier results.

Figure 38 shows receiver line 3 after the 3D raypath domain interferometry. This can be directly compared to Figure 29, where the interferometry was applied in 2D. What we notice immediately is that deeper reflections at longer offsets are stronger in Figure 38, but that overall reflection continuity seems less, particularly for shorter offsets. Figure 39 shows the 3D raypath interferometry result for receiver line 8, to be compared with Figure 31. Here, while reflections on longer-offset traces seem stronger, the reflections at near offsets actually seem weaker. We do, however, note that the residual surface wave noise has all but vanished on the 3D raypath interferometry result.

The most interesting result occurs for receiver line 17, which is nearly collinear with the source point. Figure 40 shows the 3D raypath domain interferometry result for this ensemble, which can be compared with Figure 33. The striking result is that the surface wave residual is practically gone, while reflections at all levels are significantly enhanced, even some which were formerly obscured by the residual noise. Once again, however, reflections are missing at near offsets.

Results for receiver lines 21 and 30 are shown in Figures 41 and 42, which can be compared to Figures 35 and 37, respectively. Results are similar, in that the residual noise is greatly diminished, and deeper reflections at longer offsets are enhanced. Near-offset reflections are somewhat weaker, but, at least on receiver line 30, continuous and coherent.

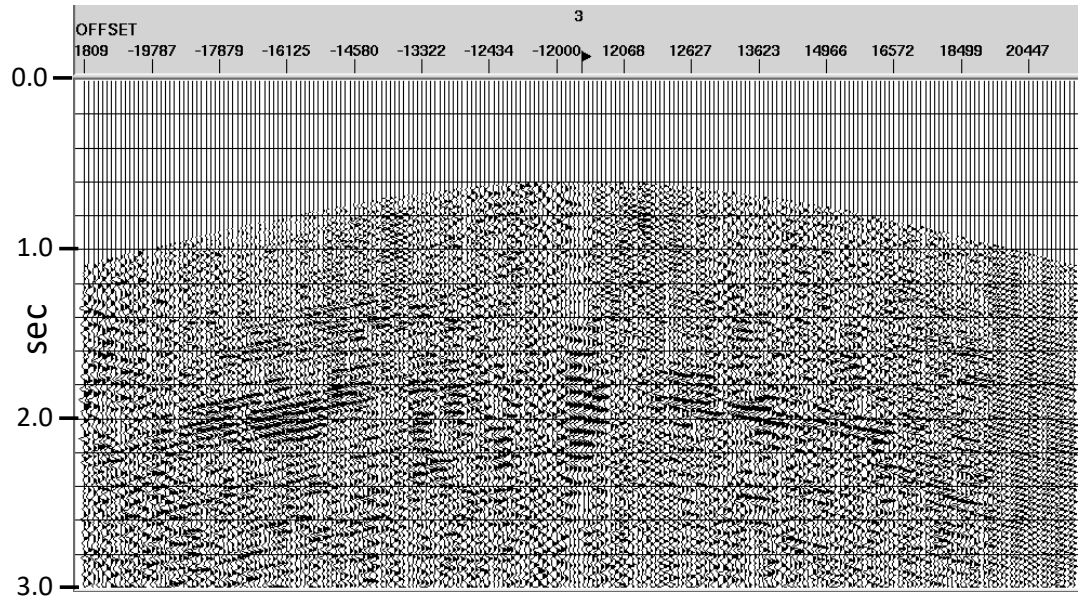

FIG. 38. Receiver line 3 after 3D raypath interferometry applied to the azimuth/offset ensembles. Compare with Figure 29.

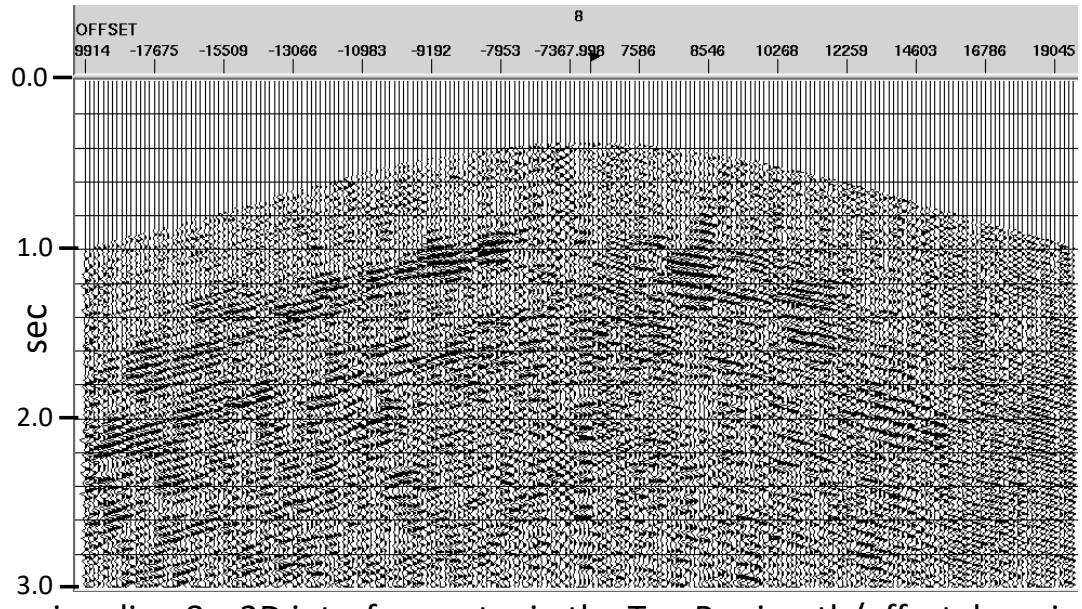

FIG. 39. Receiver line 8 after 3D raypath interferometry applied to the azimuth/offset ensembles. Compare with Figure 31.

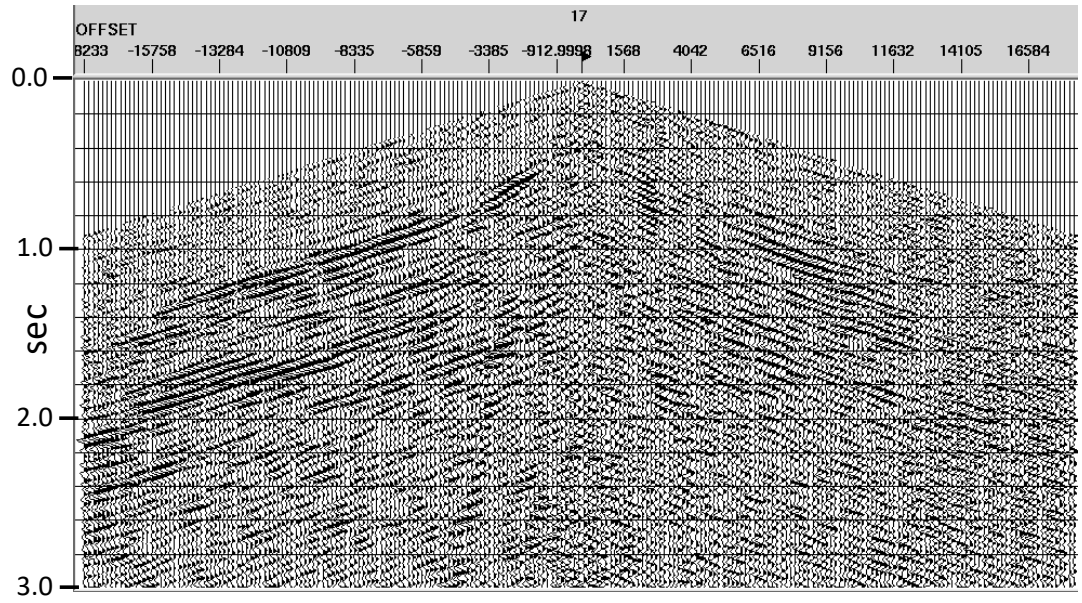

FIG. 40. Receiver line 17 after 3D raypath interferometry applied to azimuth/offset ensembles. Compare with Figure 33.

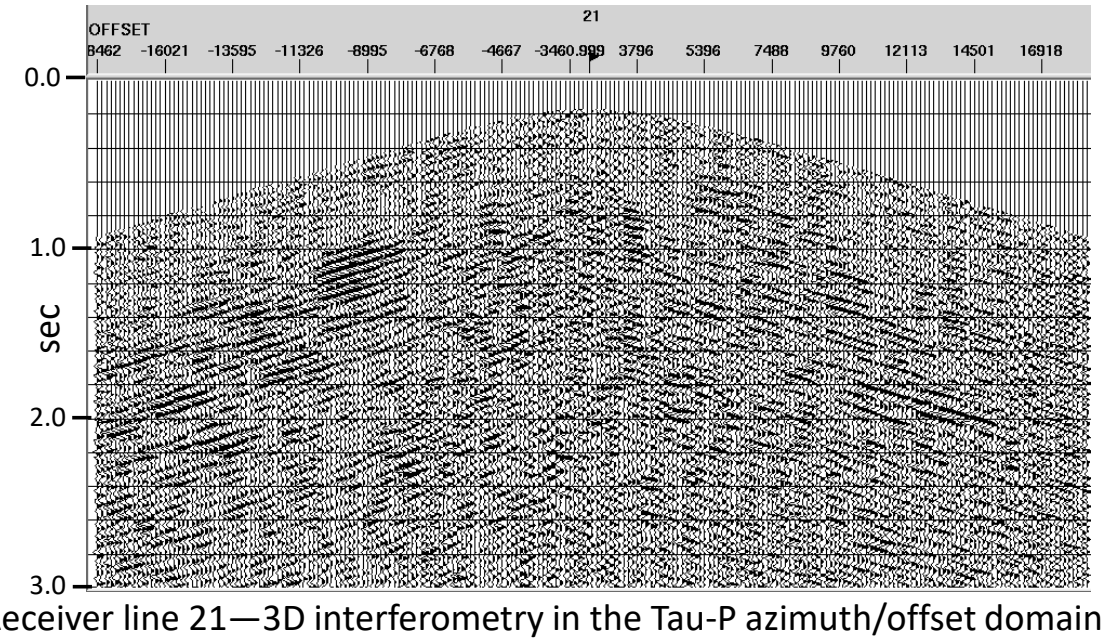

FIG. 41. Receiver line 21 after 3D raypath interferometry applied to azimuth/offset ensembles. Compare with Figure 35.

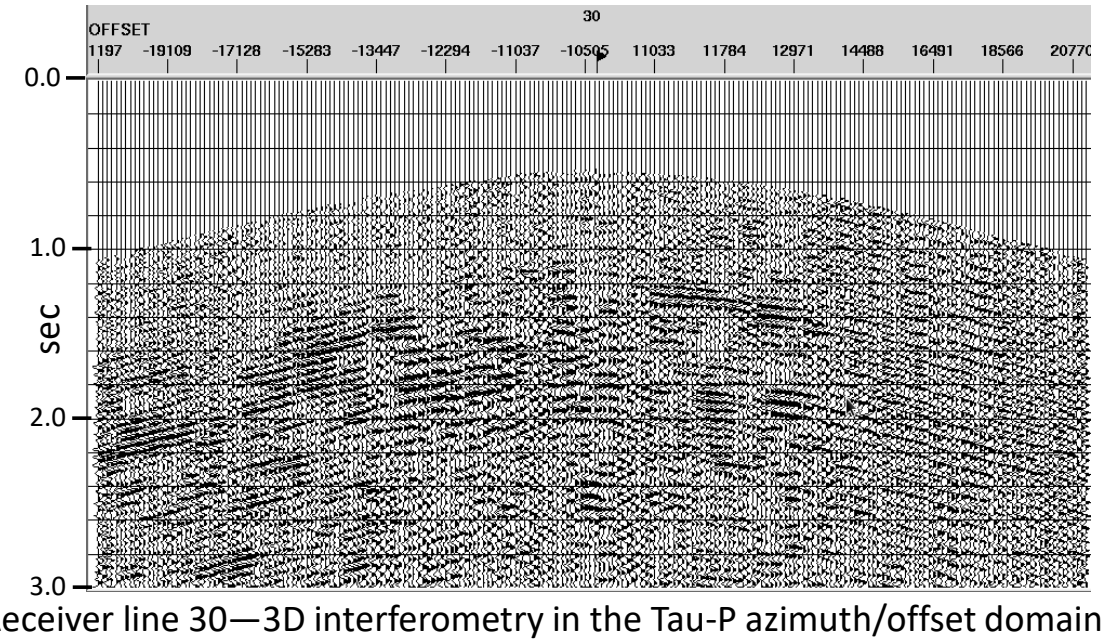

FIG. 42. Receiver line 30 after 3D raypath interferometry applied to azimuth/offset ensembles. Compare with Figure 37.

Summarizing these results; applying 3D interferometry in the azimuth/offset raypath domain provides results that are significantly different from 3D interferometry in the azimuth/receiver-line X/T domain. For one thing, the interferometry application appears to remove most of the residual surface wave noise, allowing reflections hidden by this noise to appear. Also, reflections at later times and greater offsets appear to be preferentially enhanced. A close look at some of these reflections, however, shows that they appear to 'ring' in a rather narrow-band fashion. This could be due to loss of bandwidth in the forward/inverse Tau-P transform process, or it could be related to the bandwidth of the cross-correlation functions used as match filters.

SUMMARY AND DISCUSSION

We realized that in many cases, it would not be practical to apply the full raypath interferometric near-surface correction procedure that we described previously (Henley, 2016a, 2017b) to a 3D data set of significant size. As an alternative, we have explored the possibility of using interferometry to at least partially remove near-surface effects, in a more local sense, from individual single-fold 3D source ensembles. We then envision extending the procedure to a '2.5D' full correction. Although the first interferometric procedure would be applied independently to each source gather within a 3D survey, we would expect the receiver lines of interferometrically corrected source gathers to exhibit similar appearance when source positions are near each other, since the sources would typically have the receiver lines in common, and would see very similar near-surface receiver effects. We have not fully considered the next step; but speculate that some sort of correlation between the corrected receiver line gathers of nearest-neighbour source positions should allow us to at least apply shot-to-shot corrections that would complete the near-surface corrections. In order to avoid correlating many thousands of traces just to

apply a differential correction between two source gathers, we would probably sum traces within bins first to reduce the number of shot-to-shot correlations.

Although we loosely describe a possible 2.5D near-surface correction process for 3D data, it would not be a full raypath interferometry procedure, even if we do the source gather corrections using 3D raypath interferometry, because the final step would be the differential source-to-source near-surface reconciliation, applied strictly in the X/T domain, as described above. However, since we know that the most likely need for raypath interferometry is for converted wave (PS) data with its non-stationarity requirement, applying raypath interferometry to each source gather should satisfy this requirement for the receiver-side corrections.

We looked at three different schemes for removing apparent near-surface variations from the traces of a 3D source gather, one of them a 2D approach, the others 3D, in the sense that the estimated wavefield was created by smoothing the input data in two different, nearly orthogonal directions, thus incorporating 2 dimensions. While the 2D method appeared to be most effective at improving event coherence within each receiver line gather, it was also the most susceptible to interference from residual coherent noise, probably because source-generated noise is best organized in this domain. Furthermore, each receiver line was done independently, with no operation to tie the separate sets of receiver line corrections together within the source gather. On the other hand, because we sort the traces into common-azimuth bins to apply the 3D interferometry, we are able to smooth the traces in two different directions while estimating the wavefield, thus forcing areal coherence for the estimated wavefield, rather than restricting the smoothing to receiver line direction only, as in the 2D case. When we apply the interferometry in the azimuth/offset domain, or in the azimuth/offset raypath domain, then sort traces back to receiver lines, we observe modestly improved event coherence. In this case, however, we know the effect is 3D, but the improvement nevertheless successfully projects to the 2D receiver line ensembles.

We noticed that the 3D raypath interferometry results looked more ‘narrow band’ than earlier results in the 3D X/T domain. In all likelihood, the narrowing of the band is a result of the forward/inverse Tau-P transform, with its slightly reduced fidelity. More careful attention to parameters might partially alleviate this, as would switching to the RT transform instead.

Removing the near-surface ‘wrinkles’ from 3D source gathers using modified interferometry seems promising as a less expensive alternative to applying full 3D raypath interferometry. To verify this as a useful technique, we would need to apply it to all the source gathers on a 3D survey, then concoct a source reconciliation process to apply to the processed source gathers before finally combining them via 3D CMP stacking or other imaging process.

ACKNOWLEDGEMENTS

Thanks to CREWES and NSERC for funding, and to Marianne Rauch-Davies of Devon for the 3D source ensemble used in this study.

REFERENCES

Cova, R., Henley, D.C., and Innanen, K.A.H., 2013, Non-stationary shear wave statics in the radial trace domain, CREWES Research Report, 25.

Cova, R., Henley, D.C., and Innanen, K.A.H., 2014, Making shear wave statics actual statics using radial trace and tau-p transforms, CREWES Research Report, 26.

Cova, R., Wei, X., and Innanen, K.A.H., 2015a, Shear wave near-surface corrections in the tau-p domain: a case study, CREWES Research Report, 27.

Cova, R., Henley, D.C.., and Innanen, K.A., 2015b, Addressing shear wave static corrections in the ray parameter domain: a non-stationary interferometric approach, SEG Technical Program Expanded Abstracts 2015.

Cova, R., Henley, D.C., Wei, X., and Innanen, K.A., 2017, Receiver-side near-surface corrections in the Tau-P domain: a raypath-consistent solution for converted wave processing, Geophysics, 82, No. 2, pp U13-U23.

Henley, D.C., 2004, A statistical approach to residual statics removal, CREWES Research Report, Vol. 16.

Henley, D.C., 2005, Raypath-dependent statics, CREWES Research Report Vol. 17.

Henley, D.C., 2007, Radial filtering 3D data, CREWES Research Report, 19.

Henley, D.C., 2008, Raypath interferometry: statics in difficult places, 2008, SEG Technical Program Expanded Abstracts 2008.

Henley, D.C., 2012a, Interferometric application of static corrections, Geophysics, 77, No. 1, pp Q1-Q13.

Henley, D.C., 2012b, Interference and the art of static correction: raypath interferometry at Hussar, CREWES Research Report 24.

Henley, D., 2014a, Static corrections via raypath interferometry: recent field experience: Geoconvention 2014, CSEG, Expanded abstracts 2014.

Henley, D.C., 2014b, Through a glass darkly: improving raypath interferometry, CREWES Research Report, Vol. 26.

Henley, D.C., 2015, 3D or not 3D, that is the question: raypath interferometry in 3D processing, CREWES Research Report, Vol. 27.

Henley, D.C., 2016a, To boldly go into the next dimension; 3D raypath interferometry issues, CREWES Research Report, Vol. 28.

Henley, D.C., 2016b, 3D or not 3D, that is the question: raypath interferometry in 3D processing, Geoconvention Expanded Abstracts, 2016.

Henley, D.C., 2017a, A tale of two transforms: 3D raypath interferometry, CREWES Research Report, Vol. 29.

Henley, D.C., 2017b, To boldly go into a new dimension: 3D raypath interferometry issues, Geoconvention Expanded Abstracts 2017.

Henley, D.C., Getting it right: source-receiver offsets in the radial trace transform, CREWES Research Report, Vol. 30.